

Alginate polymerization and modification by *Pseudomonas aeruginosa*: New insights into their relationship and molecular mechanism

M. Fata Moradali^a, Ivan Donati^b, Ian Sims^c, Shirin Ghods^a, Bernd H. A. Rehm^{a,d*}

^aInstitute of Fundamental Sciences, ^bDepartment of Life Sciences, University of Trieste, Trieste, Italy, ^cThe Ferrier Research Institute, Victoria University, Lower Hutt, Wellington, New Zealand, ^dMacDiarmid Institute for Advanced Materials and Nanotechnology, Massey University, Palmerston North, New Zealand

* Corresponding author: Bernd H. A. Rehm.

Address: Institute of Fundamental Sciences and MacDiarmid Institute for Advanced Materials and Nanotechnology, Massey University, Private Bag 11222, Palmerston North 4442, New Zealand. Phone:+64 6 356 9099 ext. 84704. Email: B.Rehm@massey.ac.nz.

ABSTRACT

The molecular mechanisms of alginate polymerization/modification/secretion by a proposed envelope spanning multiprotein complex are unknown. Here bacterial two-hybrid assays and pull-down experiments showed that the catalytic subunit Alg8 directly interacts with the proposed copolymerase Alg44 while embedded in the cytoplasmic membrane. Alg44 also interacted with the lipoprotein AlgK bridging the periplasmic space. Site-specific mutagenesis of Alg44 showed that protein-protein interactions and stability were independent of conserved amino acid residues R17 and R21 which are involved in c-di-GMP binding, the N-terminal PilZ domain and the C-terminal 26 amino acids. A site-specific mutagenesis approach was employed to investigate the c-di-GMP mediated activation of alginate polymerization by the PilZ_{Alg44} domain and Alg8. Activation was found to be different to the proposed activation mechanism for cellulose synthesis. The interactive role of Alg8, Alg44, AlgG (epimerase) and AlgX (acetyltransferase) on alginate polymerization and modification was studied by using site-specific deletion mutants, inactive variants and overproduction of respective subunits. The composition, molecular weight and materials properties of respective alginates was analyzed. The molecular weight was reduced by epimerization while it was increased by acetylation. Interestingly, when overproduced, Alg44, AlgG and non-epimerising variant AlgG(D324A) increased the degree of acetylation while epimerization was enhanced by AlgX and its non-acetylating variant AlgX(S269A). Biofilm architecture analysis showed that acetyl groups promoted cell aggregation. Overall this study shed new light on the arrangement of the envelope spanning multiprotein complex involved in alginate polymerization and modification. Furthermore the activation mechanism and the interplay between polymerization and modification of alginate were elucidated.

Keywords: Alginate, *Pseudomonas aeruginosa*, protein-protein interaction, polymerization

Significance statement

This study provides new insights into the molecular mechanisms of the synthesis of the unique polysaccharide, alginate, which is not only an important virulence factor of the opportunistic human pathogen *Pseudomonas aeruginosa* but which has due its material properties many application in medicine and industry. Unraveling the assembly and composition of this novel alginate synthesizing and envelope spanning multiprotein complex will be of tremendous significance for the scientific community. Due to alginates role in the pathogenesis as well as its material properties harnessed in numerous applications, this work will attract interest from a broad scientific community. Results obtained in this study will aid the design and development of inhibitory drugs as well as the commercial bacterial production of “tailor-made” alginates.

INTRODUCTION

Pseudomonas aeruginosa is an opportunistic human pathogen which can become life-threatening in immunocompromized patients. It is the leading cause of morbidity and mortality in Cystic Fibrosis patients. This is mainly due to its ability to colonize lungs by forming structured biofilms which consist of bacterial cells embedded in a complex matrix predominantly composed of alginate. Bacterial cells in biofilms are protected against the immune system and antibiotics (1, 2). Alginates are anionic exopolysaccharides composed of variable proportions of 1,4-linked β -D-mannuronic acid (M) and its C5 epimer α -L-guluronic acid (G). The alginate derived from *P. aeruginosa* is naturally acetylated and lacks consecutive G residues (GG-blocks) (3). Alginates exhibit unique gel-forming properties suitable for numerous medical and industrial applications (3, 4). The alginate structure strongly impacts its materials properties. Hence, development of bionengineering approaches to control the alginate structure will enable production of alginates with new material properties towards novel applications.

For many years *P. aeruginosa* has been the model organism to study various aspects of alginate biosynthesis such as e.g. alginate polymerization, epimerization, acetylation, secretion and regulation. Thirteen proteins are directly involved in the biosynthesis of alginate and except for *algC* their encoding genes are clustered in the alginate biosynthesis operon (*algD*, *alg8*, *alg44*, *algK*, *algE*, *algG*, *algX*, *algL*, *algI*, *algJ*, *algF*, *algA*) (5, 6). Except for soluble cytoplasmic proteins AlgA, AlgC and AlgD which are responsible for providing the activated nucleotide sugar precursor, GDP-mannuronic acid, proteins encoded by the operon are proposed to constitute an envelope spanning multiprotein complex. Two cytoplasmic membrane-anchored proteins, the glycosyltransferase, Alg8, and the proposed copolymerase, Alg44, are necessary for alginate polymerization (7-9). The MucR sensor protein, a diguanylate cyclase (DGC)/phosphodiesterase (PDE) embedded in the cytoplasmic membrane was proposed to provide c-di-GMP for binding to the cytoplasmic PilZ domain of Alg44 by which alginate polymerization is activated (10). Translocation of nascent alginate across the periplasm is coupled with modification processes including *o*-acetylation and epimerization. O-acetylation is independently catalyzed by AlgJ and AlgX (11) while the acetyl group donor is provided by AlgI

and AlgF (12, 13). The AlgG epimerase converts M residues to G residues in the nascent alginate chain. AlgG, AlgX and AlgK were suggested to form a periplasmic scaffold for guiding alginate through the periplasm for secretion via the outer membrane protein AlgE (14-18). It was also suggested that if alginate is misguided into the periplasm then degradation would be mediated by the periplasmic AlgL lyase (19).

Previous studies on protein-protein interactions and mutual stabilities of proposed subunits of the multiprotein biosynthesis machinery provided evidence of binary protein interactions including AlgE-AlgK, AlgX-AlgK, AlgX-MucD (a serine protease), Alg44-AlgX and Alg8-AlgG (20, 21). However more experimental evidence is needed to map all protein-protein interactions within the multiprotein complex in particular towards unraveling the molecular mechanisms of alginate polymerization, molecular weight control and the relationship of modification events to polymerization.

In this study, protein-protein interactions within the multiprotein complex were investigated using the bacterial two hybrid technique and pull down assays. The proposed interacting protein surface of Alg44 was probed and the molecular mechanism of c-di-GMP mediated activation was studied (22, 23).

The role of Alg8, Alg44, AlgG and AlgX with respect to polymerization and modification was studied by analyzing the composition and material properties of alginates produced by various strains. We employed a constitutively alginate producing strain *P. aeruginosa* PDO300 to generate isogenic single- and double-gene knockouts of *alg8*, *alg44*, *algG* and *algX*. This allowed studying the role of the respective proteins in alginate polymerization and/or modifications by introducing additional copy numbers of subunits or their variants *in trans*. The impact of various alginate structures on motility, biofilm formation and architecture was investigated.

Results

Protein-protein interaction of membrane-anchored Alg8 and Alg44 towards constitution of an active alginate polymerase subunit. The two cytoplasmic membrane-anchored proteins Alg8 and Alg44 were previously shown to be necessary for alginate polymerization. Alg8 is a glycosyltransferase catalyzing alginate polymerization using substrate GDP-mannuronic acid and the c-di-GMP-binding PilZ domain containing Alg44 was proposed as copolymerase (9, 24). However, the functional and structural interaction of Alg8 and Alg44 had not been elucidated. Therefore, the marker-free isogenic double-gene knockout mutant PDO300 Δ *alg8* Δ *alg44* was generated. This mutant lost the mucoid phenotype while introduction of plasmid pBBR1MCS-5:*alg44:alg8* restored alginate production and the mucoid phenotype.

In order to investigate the proposed interaction of Alg8 and Alg44, functional his-tagged variants (Alg44-6his and Alg8-6his) were subjected to pull down experiments under native conditions and to bacterial two-hybrid system assays. In pull down experiments, wild-type Alg44 and Alg8 without his-tag served as negative controls. To address possible stoichiometric effects i.e. effects of increased copy numbers of individual subunits on the integrity of the multiprotein

complex, single genes encoding Alg8-6his or Alg44-6his under the control of their native promoter were integrated into the genome. In contrast, *in trans* genes were present on plasmids in multiple copies under control of the strong constitutive *lac* promoter. Immunoblots showed that Alg44 with an apparent molecular weight of 41.8 kDa was co-purified with Alg8-6his produced either from *in trans* or *in cis* encoding genes and similarly Alg8 (~53 kDa) was co-purified with Alg44-6his while respective proteins were not detected for complemented mutants with native Alg44 and Alg8 as well as in double knockout mutants with single Alg8-6his or Alg44-6his (Fig. 1A and B).

In addition the bacterial two-hybrid system showed that the chimeric enzyme adenylate cyclase was re-constituted when its two complementary fragments (T18/T25) were brought together by Alg8 and Alg44 interaction. β -galactosidase activity in those cells harboring two plasmids producing fusion proteins of Alg8 and Alg44 (pKNT25:*alg8*+pUT18:*alg44*) was on average 11-fold [672 U/mg of cellular dry weight] greater than the negative controls without the fusion protein partner (background control) or when compared with single fusion protein Alg8 or Alg44 [58-66 U /mg of cellular dry weight] as well as the *vice versa* combination (pKNT25:*alg44* + pUT18:*alg8*) which showed a β -galactosidase activity of 160 U/mg of cellular dry weight (Fig. 1C). Analysis of cytoplasmic membrane proteins by immunoblotting confirmed that both proteins were localized to the cytoplasmic membrane of *E. coli* (Fig. 1D). These results provided the first experimental evidence for the direct interaction between the membrane-anchored proposed alginate polymerase (glycosyltransferase) Alg8 and the co-polymerase Alg44.

Cytoplasmic membrane-anchored Alg44 interacts with outer membrane-anchored AlgK while Alg44 is critical for structural integrity of the multiprotein alginate biosynthesis machinery. To assess whether Alg8 and Alg44 interact with other proposed subunits of the multiprotein complex, pull down assays under native condition were employed using Alg8-6his and Alg44-6his proteins followed by immunoblotting using anti-AlgX, -AlgK and -AlGE antibodies. Additionally, to rule out indirect interactions, appropriate double-gene knockout mutants harboring individual genes *in trans* (PDO300 Δ *alg8* Δ *alg44*(pBBR1MCS5:*alg8*), PDO300 Δ *alg8* Δ *alg44*(pBBR1MCS5:*alg44*), PDO300 Δ *alg44* Δ *algX*(pBBR1MCS5:*alg44*)) were included. To address stoichiometric effects, complemented PDO300 Δ *alg8* and PDO300 Δ *alg44*, respectively, were used to generate single gene copy complementation strains by integrating *alg8-6his* or *alg44-6his* into the bacterial genome, respectively. The mutants producing native Alg8 and Alg44 proteins were used as negative controls.

Resultant immunoblots (Fig. 2A and B) showed AlgK and AlgX but not AlGE were independently pulled down with Alg44-6his, both when *alg44-6his* was provided *in trans* or *in cis*. Hence, experimental evidence is provided as previously proposed (20) that a protein-protein interaction network spanning the periplasm and constituted by Alg8-Alg44-AlgK-AlGE interactions exists.

Crosslinking experiments using DSG cross-linking reagent with spacer arm length of 7.7 Å followed by Alg44-6his pull down under denaturing condition showed a protein with an apparent molecular weight of 84 kDa which was only detected by the anti-Alg44 antibody. In addition the previously shown Alg44-AlgX (20) interaction was confirmed by detecting a cross-linked protein with an apparent molecular weight of 90 kDa binding both anti-Alg44 and anti-AlgX antibodies. The 84 kDa protein was only detected in pull down elution fractions obtained from genomic expression of *alg44-6his*, but not from the plasmid borne gene, while Alg44-AlgX interactions were found to be independent of the stoichiometry of the individual proteins (Fig. 2C and D). These proteins were not detected in elution fractions when the native protein Alg44 was present and in the negative control treated with DMSO.

Alg44 variants with truncated PilZ domain and C-terminus were stable and maintained integrity of protein-protein interactions within the alginate biosynthesis multiprotein complex. Previously it was demonstrated that site-directed mutagenesis of the putative c-di-GMP-binding motifs (R17xxxR21) of the PilZ domain and a C-terminal truncation of Alg44 completely abolished alginate production (25). In comparison, it was shown that c-di-GMP binds directly to both PgaC and PgaD, the two cytoplasmic membrane components of the *E. coli* poly-β-1,6-N-acetylglucosamine synthesis machinery, which stimulated their glycosyltransferase activity by stabilizing their interaction (26). Here it was investigated whether c-di-GMP binding to the PilZ domain of Alg44 and the C-terminal part itself impact on protein-protein interactions and ultimately alginate polymerization.

His-pull down experiments under native condition as described above were applied using his-tagged Alg44 variants (Alg44 (R21D), Alg44 (Δ 40-74aa_{PilZ}) and C-terminally truncated Alg44 (Δ 364-389aa)) (Fig. 3A). As shown in Fig. 3B, Alg44-6his variants were all found in the envelope fraction which suggested their localization and stability was not affected. Interestingly, the abovementioned protein interaction network was confirmed which signifies neither protein stability nor the interaction of Alg44 with Alg8, AlgK and AlgX were disrupted by its defective PilZ domain and the C-terminal truncation (Fig. 3C-E).

C-di-GMP levels and growth mode impact on Alg44 stability. Previous studies showed that introducing high copy numbers of *mucR* in PDO300 Δ *mucR* resulted in greater production of alginate than found in the wild-type while increased copy numbers of *rocR* encoding a c-di-GMP degrading phosphodiesterase (PDE) led to strongly reduced alginate production presumably due to reduction in c-di-GMP levels. Therefore it was suggested that MucR plays a specific role in the regulation of alginate biosynthesis by co-localizing with Alg44 and providing a localized c-di-GMP pool (10). Here it was tested if Alg44 copy numbers in the envelope fraction might be affected by presence or absence of MucR and RocR, respectively, i.e. by different c-di-GMP levels and within different physiological conditions such as planktonic and biofilm growth modes. Immunoblotting analysis of envelope fractions of the various mutants showed the amount of Alg44 was not significantly affected by MucR absence in biofilm mode while it was reduced

in envelope fraction of biofilm cells with high copy number of *rocR* in the absence of MucR (Fig. 4), indicating that the low amount of Alg44 corresponded with low c-di-GMP levels. However the amount of Alg44 in the same mutants growing in planktonic mode did not significantly differ.

Is alginate polymerization controlled by an autoinhibition mechanism as shown for the bacterial cellulose synthase? Alg8 and BcsA of bacterial cellulose synthase both belong to the glycosyltransferase family-2 (GT-2) and they share the same conserved signature motifs and residues experimentally known as critical for production of alginate and cellulose, respectively (27, 28). Recently, the structure of bacterial cellulose synthase BcsA-BcsB complex was resolved. It was shown that PilZ domain in this complex was in proximity to the catalytic site of BcsA (28). The first arginine of PilZ domain's R580xxxR584 motif formed a salt bridge with E371 preceding the RW motif (a signature of glycosyltransferase-2 family), consequently tethering the gating loop in the resting status and blocking the catalytic site. This steric hindrance was called autoinhibiting mechanism which was proposed to be eliminated upon c-di-GMP binding to R580 opening up the gate for precursors to enter into the catalytic site.

Accordingly, an *in silico* hybrid of Alg8 and PilZ_{Alg44} informed by BcsA-BcsB structure and implementing bioinformatics analysis using the Phyre2 Protein Fold Recognition Server was designed (29). A structural model homologous to BcsA (confidence: 100%, coverage: 93%) showed the PilZ domain in proximity to the catalytic site of Alg8 and close to the residues E322, H323 and E326 located on BcsA-homologous loop preceding motif RW(339-340), a site potentially involved in salt bridge formation (Fig. 5A-C). The impact of alanine substitutions of these residues individually and in combination with R17 and/or R21 of Alg44's RXXXXR (17-21) motif at different c-di-GMP levels (i.e. presence or absence of overproduced c-di-GMP degrading RocR) on *in vivo* activity of respective Alg8 and Alg44 variants was assessed. Overproduction of RocR was confirmed to significantly reduce alginate production in wild-type strain and complemented mutants. Substitution of R residues in PilZ_{Alg44} domain's RXXXXR motif (17-21) and E322 residue of Alg8 with alanine, respectively, completely abolished alginate production. The mutagenesis of H323 (i.e. PDO300 Δ *alg8* (pBBR1MCS-5:*alg8*(H323A))) lowered alginate production by 6.9-fold when compared to PDO300 Δ *alg8* (pBBR1MCS-5:*alg8*). Interestingly, RocR mediated reduced intracellular c-di-GMP levels restored alginate production to PDO300 Δ *alg8* (pBBR1MCS-5:*alg8:rocR*) levels. Replacement of E326 by alanine in Alg8 increased alginate production by 1.3-fold compared with PDO300 Δ *alg8* (pBBR1MCS-5:*alg8*) (Fig. 5D). RocR production in this mutant background mediated decreased alginate production by about 2-fold when compared to wild-type Alg8.

The role of Alg8, Alg44, AlgG and AlgX on alginate composition and molecular weight. In order to investigate the relationship between alginate polymerization and modification, single- and double-gene knockout mutants of *P. aeruginosa* PDO300 were generated and followed by individual and combinatorial *in trans* complementation using relevant genes including

alg8/alg44 (encoding alginate-polymerizing proteins), *algX/algX(S269A)* (encoding alginate-acetylating/non-acetylating AlgX) and *algG/algG(D324A)* (encoding alginate-epimerizing/non-epimerizing AlgG). Generated knockout mutants lost mucoidity while mucoidity was restored upon *in trans* complementation with relevant genes. In order to shed light on the functional interaction between alginate-polymerizing and modifying subunits the polymerization degree, epimerization degree and acetylation level of resulting alginates were assessed. The composition and the molecular weights of the respective alginates are summarized in Table 1. Fig. 6A shows in descending order the values obtained in regard to epimerization, acetylation, polymerization degree and alginate yield. ¹H-NMR spectra of compositional analysis of alginates are shown in Fig. S1. In order to investigate whether Alg8 and Alg44 are directly involved in polymannuronate synthesis, additional copies of both Alg8 and its interacting partner Alg44 were introduced into respective mutant backgrounds. Additional copies of Alg8 and/or Alg44 had a similar effect on alginate production such as resulting in high molecular weights with reduced epimerization and acetylation when compared to the wild-type control (Fig. 6A, Table 1). The same effect of Alg8 and Alg44 on alginate polymerization supported the hypothesis that both subunits constitute the alginate polymerase.

AlgF, AlgI and AlgJ were proposed to form a protein complex constituting the alginate acetyltransferase/acetylase (12, 30, 31). Recently, AlgX was demonstrated to play a role in alginate acetylation. AlgX is a two-domain protein including a domain with acetyltransferase activity and a carbohydrate-binding domain. Replacement of amino acid residues S269-H176-D174 which were proposed to constitute the catalytic site resulted in non-acetylated alginate (13). AlgG, the epimerase contains a conserved DPHD motif (residues 324-327) (14, 32, 33), the proposed active site involved in epimerization. Replacement of amino acid residues in this motif was shown to result in non-epimerized alginate while modified AlgG retained its protective role on nascent alginate against degradation in the periplasm. Here we used catalytically inactive variants of AlgX (S269A) and AlgG (D324A). When only the inactive AlgX variant was present, the resulting alginate was non-acetylated. Interestingly, additional copies of active AlgX or inactive AlgX resulted in the highest epimerization values of $F_G = 0.36$. Additional copies of both AlgG and AlgX or inactive variants respectively, increased the degree of epimerization of the resulting alginate (Fig. 6A). Additional copies of both AlgX and AlgG increased the degree of acetylation when compared to additional copies of only AlgX (Fig. 6A). Interestingly, additional copies of Alg44 enhanced acetylation 2.7-fold when compared to AlgX.

The correlation between molecular weight of alginate and alginate modification such as acetylation and epimerization was assessed (Fig. 6B). The molecular weight of the various alginates was determined by SEC-MALLS (Fig. S2). The highest degree of polymerization ($4653 \pm 1.1\%$ kDa corresponding to about 22876 uronic acid residues) was detected in alginates from strains with additional copies of the catalytically inactive epimerase variant AlgG (D324A). This was an about 69% increase in molecular weight when compared to alginate produced from strains with additional copies of epimerizing AlgG. The lowest molecular weight alginates were produced by strains harboring additional copies of those subunits contributing the highest levels

of epimerization i.e. AlgX ($F_G = 0.36$), AlgX (S269A) ($F_G = 0.36$) along with the lowest levels of acetylation (9.8% and 0). Non-acetylated and non-epimerized alginates ($F_G = 0$, Ac. = 0%) showed the lowest molecular weight ($1811 \pm 0.9\%$ kDa). Since $^1\text{H-NMR}$ spectra of the various alginates did not detect double bonds a result of alginate lyase mediated degradation, the alginate lyase presumably did not influence the polymerization degree. As a result of alginate lyase mediated degradation of alginate a double bond is formed between the C4 and C5 carbons leading to 4-deoxy-L-erythro-hex-4-enopyranosyluronic acid containing non-reducing terminal moiety which can be clearly detected by $^1\text{H-NMR}$ analysis. Additional copies of Alg8 and Alg44 gave rise to increased molecular weights ranging 3000 to 3800 kDa supporting their direct involvement in alginate chain synthesis. These data suggested that the alginate molecular weight is inversely correlated with alginate epimerization but positively correlated with acetylation (Fig. 6B). Alginates produced by the various strains showed a narrow molecular weight distribution with a polydispersity index close to 1 (Table 1).

***In vivo* alginate polymerase activity.** Alginate produced by the various strains was isolated and quantified (Fig. 6C). Although additional copies of the various proteins increased the amount of produced alginate when compared to the reference strain PDO300 (pBBR1MCS-5), a significant variation of alginate productivity, i.e. alginate polymerase activity, was detected. Interestingly, additional copies of non-acetyating AlgX (S269A) and native AlgX mediated production of the largest amounts of alginate while epimerizing and non-epimerizing AlgG mediated the lowest level of production (Fig. 6C). Pairwise comparison of these four strains showed that more alginate is produced in the absence of modification events. The enhancing role of AlgX in alginate production was further supported when additional copies of AlgX together with AlgG led to a strong production of alginate. However, the non-acetyating and non-epimerizing pair of them resulted in a much lower quantity (Fig. 6C). Furthermore, all attempts to restore alginate production in PDO300 Δ alg44 Δ algX with pBBR1MCS-5:alg44:algX failed. The mucoid phenotype of this double-gene knockout mutant was only restored when one of the introduced complementing genes, either *alg44* or *algX*, were integrated into the genome (*in cis* complementation using mini-CTX) and the other one presented *in trans* resulting in alginate production of 1.9 g /g CDM).

Microrheological analysis of various alginates. Particle-tracking microrheology was applied to assess the viscoelastic properties of the various alginates. All alginates showed viscoelastic properties in which the solid-like elastic modulus G' was greater than the liquid-like viscous modulus G'' ($G' > G''$). The plot of particles mean square displacement (MSD) versus correlation time showed MSD curves of the alginates are distributed in four distinct categories (Fig. S3). In the first category, the alginates produced from PDO300 Δ algG (pBBR1MCS-5:algG(D324A)) and PDO300 Δ alg8 (pBBR1MCS-5:alg8), respectively, without G-residues and with the highest molar fraction of MM-blocks, and both with very high molecular weight, showed the highest and quite similar viscoelastic properties ($G' = 0.41$, $G'' = 0.3$; $G' = 0.40$, $G'' = 0.28$, respectively).

Interestingly, the alginates from PDO300 Δ *alg44* (pBBR1MCS-5:*alg44*), PDO300 Δ *algG* (pBBR1MCS-5:*algG*) and PDO300 (pBBR1MCS-5) dropped into the second category with lower viscoelastic property. In the third category showing lower viscoelastic property, those alginates with molecular weight of ≤ 2000 kDa produced by PDO300 Δ *algX* (pBBR1MCS-5:*algX*(S269A)) and PDO300 Δ *algX* Δ *algG* (pBBR1MCS-5:*algX*(S269A): *algG*(D324A)) were found. Surprisingly, acetylated alginate from PDO300 Δ *algX* (pBBR1MCS-5:*algX*) was the only member of fourth category with the lowest viscoelastic property among all analyzed samples. These results suggested that viscoelasticity was positively impacted by the molecular weight combined with high M content while G-residue and acetyl group presence in the alginate chain lowered viscoelasticity. All these polymers showed greater elasticity than viscosity ($G' > G''$).

The impact of various alginates on biofilm formation. *P. aeruginosa* is capable of different modes of motilities such as twitching, swarming and swimming which are controlled by various regulatory pathways and environmental factors as well as play an important role in biofilm formation and dispersal. Here motility assays were conducted with strains capable of producing different alginates in order to assess the relationship between alginate composition/molecular weight, i.e. material properties, and motility ultimately impacting on biofilm formation (Fig. 7). All strains with alginate production greater than PDO300 (pBBR1MCS-5) showed lower twitching motility while non-alginate producing knockout mutants showed greater twitching values. The lowest twitching motility among all strains was found for PDO300 Δ *alg44* (pBBR1MCS-5:*alg44*). Twitching motility differences between PDO300 Δ *algX* (pBBR1MCS-5:*algX*) and PDO300 Δ *algX* (pBBR1MCS-5:*algX*(S269A)) or between PDO300 Δ *algG* (pBBR1MCS-5:*algG*) and PDO300 Δ *algG* (pBBR1MCS-5:*algG*(D324A)) were insignificant (Fig. 7).

Swarming motility which occurs on semi-solid surfaces and is regulated by quorum sensing was assessed as being lower in alginate producing strains than in their respective knockout mutants except for PDO300 Δ *alg8* (pBBR1MCS-5:*alg8*) which showed slightly greater swarming motility than PDO300 Δ *alg8* (pBBR1MCS-5). Among alginate-producing strains, the greatest value of swarming motility was found for strains PDO300 Δ *alg44* (pBBR1MCS-5:*alg44*) (11.33 mm) and PDO300 Δ *algX* (pBBR1MCS-5:*algX*) (11.0 mm). PDO300 Δ *algG* (pBBR1MCS-5:*algG*(D324A)) (6.83 mm) showed slightly greater swarming motility than PDO300 Δ *algG* (pBBR1MCS-5:*algG*) (6.0 mm).

Swimming which occurs in aqueous environments was tested and obtained values from swimming assays significantly varied among strains. Generally, alginate producing strains showed lower swimming capability than knockout mutants except for the mutants PDO300 Δ *alg8* (pBBR1MCS-5:*alg8*) and PDO300 Δ *alg8* (pBBR1MCS-5) (Fig. 7).

Confocal laser scanning microscopy images of biofilms formed by mutant PDO300 Δ *algX* (pBBR1MCS-5:*algX*) and its non-acetylating counterpart, PDO300 Δ *algX* (pBBR1MCS-5:*algX*(S269A)) highlighted the crucial role of acetylation of alginate for developing biofilms and cellular arrangements (Fig. S4). Comparison of the two strains revealed significant

differences in elevated structures and the distribution of microcolonies such as the structures formed by strains producing acetylated alginates which were perfectly shaped and developed with a biovolume of $5.5 \pm 1.26 \mu\text{m}^3/\mu\text{m}^2$ and a maximum height of $83 \mu\text{m}$ while those formed with non-acetylated alginate showed a smaller biovolume of $3.9 \pm 0.2 \mu\text{m}^3/\mu\text{m}^2$ and a reduced height of $26 \mu\text{m}$ with irregular architecture. Interestingly, the strain producing acetylated alginate did not produce multicellular base layer and cells were organized in pillar-shaped architectures similar to structures described for the architectures of Psl-overproducing strain (i.e. *P. aeruginosa* WFP801) (34, 35). In contrast, the strain producing non-acetylated alginate formed a biofilm with disordered and scattered microcolonies (Fig. S4, frame 3). Furthermore, PDO300 Δ algX (pBBR1MCS-5:algX) formed a biofilm with 1.5-fold more compactness and 31% more live cells than the biofilm formed by PDO300 Δ algX(pBBR1MCS-5:algX(S269A)) (Table 2). PDO300 Δ algX(pBBR1MCS-5) mutant did not form a structured biofilm but a multicellular layer with a thickness of $6 \mu\text{m}$.

PDO300 Δ algG (pBBR1MCS-5:algG(D324A)) which produced high molecular weight acetylated polymannuronate with strong viscoelasticity acquired the largest biovolume of $6.0 \pm 0.22 \mu\text{m}^3/\mu\text{m}^2$ (Fig. S5). Interestingly, adjacent structures were networked with horizontal appendages and void spaces and channels formed underneath whole structures, likely to constitute water channels. On the other hand, PDO300 Δ algG (pBBR1MCS-5:algG) which produced lower molecular weight acetylated and G residue containing alginate formed elevated but less developed structures with less biovolume of $4.8 \pm 0.22 \mu\text{m}^3/\mu\text{m}^2$ (Fig. S5). The base layers formed by both strains were dense and covered the whole area of the surface. The biofilm of PDO300 Δ algG (pBBR1MCS-5) was a homogenous layer of cells ($7 \mu\text{m}$ thickness) without elevated structures (Fig. S5).

PDO300 Δ algG Δ algX (pBBR1MCS-5: algX(S269A):algG(D324A)) produced a non-acetylated polymannuronate with a low molecular weight and the respective biofilm was composed of very long and narrowly elevated structures (Fig. 8). The biovolume was $1.5 \pm 0.2 \mu\text{m}^3/\mu\text{m}^2$ which was less than for all the other investigated strains.

Strains PDO300 Δ alg8 (pBBR1MCS-5:alg8) and PDO300 Δ alg44 (pBBR1MCS-5:alg44) established heterogeneous highly structured biofilms (Fig. S6). The former formed a biovolume of $3.95 \pm 0.43 \mu\text{m}^3/\mu\text{m}^2$ and compactness of 6.09×10^2 while the latter generated very dense and large structures with biovolume of $5.8 \pm 0.43 \mu\text{m}^3/\mu\text{m}^2$ but less compactness (4.43×10^2). Both mutants showed higher numbers of dead cells among all applied mutants but less than wild-type (Table 2). Conversely, PDO300 Δ alg8 (pBBR1MCS-5) and PDO300 Δ alg44 (pBBR1MCS-5) generated homogenous biofilm without elevated or highly structured architectures. Compactness values and dead/live ratios are summarized in Table 2.

Discussion

In this study we investigated the relationship between alginate polymerization and modification, the functional role of the subunits Alg8, Alg44, AlgG and AlgX and their physical and functional interaction. A range of alginate compositions and molecular weights exhibiting various material

properties were produced by engineered *P. aeruginosa* strains and their impact on motility and biofilms formation was assessed. Alg8 had been proposed as alginate polymerase to catalyze the transfer of mannuronic acid residues from the donor GDP-mannuronic acid to a growing acceptor molecule (25, 36). Alg44, the c-di-GMP perceiving proposed copolymerase was found to be essential for alginate polymerization. Disruption of the c-di-GMP binding site of PilZ_{Alg44} domain confirmed this critical allosteric function in regulation of alginate polymerization (8, 25). In this study, the physical and functional interaction of membrane anchored Alg8 and Alg44 was analyzed. Single- and double-gene knockout mutant of *alg8* and *alg44* were generated and alginate production was restored in these mutants by *in trans*- or *in cis*-presence of the respective deleted genes. His-tagged variants of either Alg8 or Alg44 enabled the co-purification of interacting proteins confirming a protein-protein interaction between Alg8 and Alg44 (Fig. 1). In addition, the bacterial two hybrid system was used which further confirmed the interaction of Alg8 and Alg44 in the cytoplasmic membrane (Fig. 1). However, pull down experiments also revealed that Alg44 is interacting with AlgK (Fig. 2A) which is an outer membrane lipoprotein that aids correct localization of the AlgE porin in the outer membrane. Since Alg44 had also been reported to interact with AlgX, Alg44 might play a critical role for the functional integrity of the envelope spanning alginate producing multiprotein complex. This study provides experimental evidence for the previously suggested (20) presence of the Alg8-Alg44-AlgX-AlgK-AlgE multiprotein complex bridging the periplasm from cytoplasmic to outer membrane forming the alginate polymerization/modification secretion machinery. Additionally, immunoblotting of chemically cross-linked envelope fractions using his-tagged Alg44 for pull down experiments suggested that Alg44 forms a dimer (Fig. 2C and D). Bioinformatics analysis of the periplasmic part of Alg44 suggests the presence of coil-coiled structure (Coil/Pcoils-based score: 0.4) which have been described for membrane fusion proteins (MFPs) such as MexA and polysaccharide copolymerases (PCPs) to contribute to oligomerization (37-40). The functional role of the C terminus and c-di-GMP binding of Alg44 on protein-protein interactions i.e. multiprotein complex integrity was addressed by site-specific mutagenesis. Interestingly, these Alg44 variants were stable and localized to the envelope fraction while sustaining the protein interaction network (Fig. 3). Neither Alg44 stability nor the interaction of Alg44 with Alg8, AlgK and AlgX were disrupted by its defective PilZ domain and C-terminal truncation (Figure 3C-E). These experiments suggested Alg44 mediates a different activation mechanism as was found for the PgaCD complex whose protein-protein interaction failed in the absence of c-di-GMP (26). In addition the absence or presence of a localized intracellular c-di-GMP pool did not impact the stability of Alg44 suggesting that c-di-GMP activation does not occur via stabilization of Alg44 (Fig. 4).

Therefore, it was assessed whether c-di-GMP binding to Alg44 and the resulting activation of alginate polymerization was more likely to resemble the activation mechanisms recently proposed for BcsA-BcsB cellulose synthase complex where c-di-GMP binding releases an autoinhibited state by breaking a salt bridge that sequesters a conserved gating loop that blocks access of substrate to the active site (22). Removal of this salt bridge by mutagenesis

locked the cellulose synthase in an active state. An alignment of Alg8 with BcsA and 3D model of an *in silico* constructed Alg8-PilZ fusion protein simulating the BcsA structure indicated 3 candidate amino acid residues (E322, H323, E326) for salt bridge formation (Fig. 5 A-C). These residues were replaced by alanine, respectively. These residues are highly conserved among homologous bacterial *alg8* genes but absent in homologous algal genes (Esi0010_0147 and Esi0086_0005). Replacement of R residues of PilZ_{Alg44} domain's RXXXR (17-21) individually and in combination with other mutations of Alg8 abolished alginate production (Fig. 5D). In contrast to wild-type Alg8 alginate synthesis was increased for variant Alg8 (H323A) at reduced c-di-GMP levels. This result indicated that residue H323 might be involved in c-di-GMP-dependent activation of alginate polymerase. In Phyre2 model H323 was located in the loop preceding the highly conserved Alg8's RW motif (Fig. 5 A-C). H323 is highly conserved among bacterial Alg8s. Overall, these results suggested that alginate polymerization might not be governed by a cellulose synthase-associated autoinhibiting mechanism (41).

First experimental evidence was obtained that AlgX and AlgG exhibit a mutually auxiliary behavior suggesting that the two modification events (acetylation, epimerization) are not competitive and linked (33, 42). In addition we propose a new auxiliary role for Alg44 in acetylation besides being necessary for c-di-GMP dependent activation alginate polymerization (Table 1, Fig. 6A). Failed attempts in complementing PDO300 Δ *alg44* Δ *algX* with pBBR1MCS-5:*alg44:algX* but successful complementation when one gene was *in cis* and another was *in trans* suggested that the stoichiometry of these two proteins is critical for proper performance of the multiprotein complex.

In order to shed light on how alginate polymerization (Alg8, Alg44) is aligned with alginate modification (AlgG, AlgX) respective single and double knock out mutants were generated and the effect of additional gene copies on alginate synthesis and modification was analyzed (Table 1, Fig. 6). As shown in Fig. 6A, additional copies of active or inactive AlgX acetyltransferase significantly increased the molar fraction of G residues as well as productivity which appeared inversely correlated with the alginate molecular weight (Fig. 6B and C). This suggests a new role of AlgX in epimerization and as periplasmic scaffold protein playing a key role in efficient translocation of the alginate chain across the periplasm. Recently, it was reported that AlgX binds to polymannuronic acid in a length-dependent manner and acts as terminal acetyltransferase (11).

Interestingly, restoration of alginate production of the AlgG negative mutant by an inactive variant of AlgG led to a significantly increased alginate molecular weight when compared to active AlgG suggesting that AlgG as scaffold subunit is critical for processivity of alginate polymerization while the actual epimerization event interferes with processivity (Fig. 6A-C). Furthermore, the role of AlgG mediated epimerization on alginate length might be due to AlgG mediated alginate degradation as polysaccharide epimerases show a similar reaction mechanism compared to polysaccharide lyases (54). This finding might also explain why algal alginates with high molar fraction of G residues introduced by epimerases have very low molecular weights (43).

Acetylation was found to be dependent on AlgX as previously described (11, 13) with additional copies of the various studied subunit components negatively impacting acetylation degree. Acetylation was correlated with the molecular weight suggesting no impact on processivity of alginate polymerization (Fig. 6B). In general, additional copies of any subunit increased alginate production when compared to the reference strain indicating that the stoichiometry of the various subunits is less critical for the activity of the multiprotein complex (Fig. 6C). Based on these results in regard to the roles of the investigated subunits in alginate synthesis and modification a revised model of the alginate biosynthesis multiprotein complex was proposed (Fig. 9).

The various strains generated in this study produced a broad range of alginates varying in degree of acetylation, G and M residue composition as well as molecular weight. Viscoelastic analysis of these alginates showed that the highest viscoelasticity was gained when the highest molar fraction of MM-blocks was combined with the highest molecular weight. However, increasing molar fractions of G-residues caused a decline in viscoelasticity which was even stronger with increasing degree of acetylation (Fig. S3). Acetyl groups could serve as spacers between alginate chains interfering with intermolecular interactions and hence leading to lower viscoelasticity.

Motility mediated by twitching, swarming and swimming was assessed using strains producing various alginates. These motilities are critical for biofilm development and dispersal (44). Our results showed that all alginate-producing mutants had lower values of twitching motility than non-alginate producing mutants (Fig. 7). Except for PDO300 Δ *alg8* (pBBR1MCS-5:*alg8*), swarming and swimming values of other alginate-producing mutants were variably lower than those of non-alginate producing ones. Previously it was shown that high levels of c-di-GMP reduce motility while increase production of various exopolysaccharides and biofilm formation (45, 46). Here we showed overproduction of alginate interferes with motilities. PDO300 Δ *alg44* (pBBR1MCS-5:*alg44*) showed the lowest twitching motility compared to PDO300 Δ *alg44* and also to other alginate-producing and non-alginate producing mutants (Fig. 8). Type IV pili (T4P) mediate twitching or surface-associated movement which is controlled by high concentration of c-di-GMP (47). Also, complemented mutants producing alginate, except for PDO300 Δ *alg8* (pBBR1MCS-5:*alg8*), showed significant reduction in swarming motility compared with non-alginate producing mutants. Swimming ability of alginate-producing mutants was reduced but not as significant as other motilities except for PDO300 Δ *alg44* (pBBR1MCS-5:*alg44*) whose swimming motility value was significantly reduced compared with PDO300 Δ *alg44*. Moreover, our result showed these motilities are independent of acetyl group and G residue content in alginate composition.

The impact of the various alginates exhibiting a range of material properties on its biological function in regard to biofilm formation was investigated. Acetylated alginates gave rise to well-developed and highly organized heterogeneous architectures and promoted cell aggregations (Fig. S4) which was consistent with previous studies (48). These findings suggested viscoelasticity is not critical for biofilm architecture formation. Fig. S5 shows that non-

epimerized alginate (polymannuronate) with high molecular weight gave rise to 2-fold increase in biovolume of microcolonies in biofilms when compared with those formed from epimerized alginate. Additionally, these microcolonies were networked with some horizontal appendages with embedded water channels. This suggested that the strong viscoelasticity of these alginates supported the establishment of these biofilm features and that by controlling the molar fraction of G residues biofilm architecture characteristics could be adapted to various environments. The role of acetylation and epimerization events on microcolony and biofilm formation was further assessed and the lack of G-residues and acetyl groups caused the formation of undeveloped and narrow microcolonies which were supported by specific long trails or strips of cells emerging from stigmergic self-organization of cells affected by this particular alginate (Fig. 8) (49). This was further evidence for the role alginate material properties on the formation of particular biofilm architectures and cellular aggregation patterns.

This study has provided new insights into the protein interaction network constituting the *P. aeruginosa* alginate polymerization/modification/secretion complex. First experimental evidence for Alg8 and Alg44 interaction constituting the membrane embedded catalytic unit of the multiprotein complex as well as that the c-di-GMP activation mechanisms differs from the mechanisms proposed for cellulose and poly- β -1,6-N-acetylglucosamine synthesis. Site-specific mutagenesis indicated the involvement of conserved amino acid residues of Alg8 (H323 and E326) in c-di-GMP mediated activation. Analysis of alginate modification processes suggested new roles for Alg44 and AlgG in enhancing acetylation and AlgX as promoting epimerization, providing evidence for a more complex functional relationship of subunits of the multiprotein complex as previously proposed. In addition a relationship between alginate polymerization and modification (i.e. acetylation and epimerization) was discovered such as that the molecular weight of alginate was found to be inversely impacted by epimerization while acetylation was positively correlated with molecular weight. This study led to the development of production strains producing a range of alginates enabling structure-function relationship analysis from a materials property and biological function perspective such as demonstrating that viscoelasticity of alginate contributed to enhanced cell aggregation during biofilm formation.

MATERIAL AND METHODS

Bacterial strains, plasmids, growth conditions and chemicals. Strains and plasmids used in this study are summarized in Table S1. *P. aeruginosa* and *Escherichia coli* strains were cultivated in Luria Broth medium supplemented by appropriate antibiotics and were grown at 37°C. For those assays designed for studying alginate production, bacterial phenotype and protein-protein interaction and stability, Difco™ Pseudomonas Isolation Agar (PIA) medium was used which was supplemented by appropriate antibiotics. To rule out the effect of growth condition and media on alginate composition and quantity, all experiments had been conducted under the same condition and using the same batch culture at the same time. All chemicals were purchased from Sigma-Aldrich and Merck KGaA unless otherwise mentioned. All applied enzymes for cloning were manufactured by Roche, New England Biolabs GmbH or Invitrogen.

Construction of isogenic single- and double-gene knockout mutant in *alg8*, *alg44*, *algG* and *algX* genes. Following the procedure shown in Fig. 10, marker-free single- and double-gene knockout mutants PDO300 Δ *alg8* Δ *alg44*, PDO300 Δ *algG*, PDO300 Δ *algX* Δ *algG*, PDO300 Δ *alg44* Δ *algG* were generated through two events of homologous recombination using suicide plasmid pEX100T Δ *alg44* Ω Gm, pEX100T Δ *alg8* Ω Gm, pEX100T Δ *algG* Ω Gm and pEX100T Δ *algX* Ω Gm. Strains PDO300 Δ *alg8* and PDO300 Δ *alg44* were generated previously (24). These suicide plasmids containing knockout genes (only 5' and 3' flanking regions of the respective gene) which were disrupted by the *aacC1* gene (1,100-bp fragment encoding gentamicin acetyltransferase) flanked by two *FRT* sites (flippase recombinase target) (7). They were individually transferred into *E. coli* S17-1 competent cells as donor for transfer into PDO300, PDO300 Δ *alg44* and PDO300 Δ *algX*. Transconjugants were selected on mineral salt medium (MSM) containing 100 μ g/mL gentamicin and 5% (wt/vol) sucrose (50). Cells emerging from double-crossover events grew on this medium and those cells harboring suicide plasmid with counter-selectable marker, *sacB*, or undergoing single crossover events did not grow. Gene replacement was confirmed after subculture of cells on PIA medium containing 300 μ g/mL gentamicin followed by PCR with primers binding to sites outside the flanking regions of the respective target gene.

E. coli SM10 was used as donor to transfer the flippase recombinase encoding vector pFLP2 into presumable knockout mutants and after 24 h of cultivation on PIA medium containing 5% (wt/vol) sucrose, they were screened based on sensitivity to gentamicin and carbenicillin (51). Gentamicin and carbenicillin-sensitive cells were analyzed by PCR with primers *alg8* up/down, *alg44* up/down, *algX* up/down and *algG* up/down for successful loss of the *FTR-aacC1-FRT* cassette and to confirm that the target gene was deleted.

***In trans*-complementation of single- and double-gene knockout mutants.** The genes *alg8*, *alg44*, *algG* and *algX* of *P. aeruginosa* PAO1 were individually amplified by PCR and separately ligated into pGEM-T Easy vector (Promega) for sequencing. The genes *algG*(D324A) and *algX*(S269A) respectively encoding point-mutated non-epimerising AlgG and non-acetylating AlgX proteins were synthesized by GenScript. These genes were individually or simultaneously ligated into the corresponding sites of pBBR1MCS-5 (52) (cf. Table S1) resulting in the final constructs pBBR1MCS-5:*alg44:alg8*, pBBR1MCS-5:*algG*, pBBR1MCS-5:*algX*, pBBR1MCS-5:*algX:algG*, pBBR1MCS-5:*alg44:algG*, pBBR1MCS-5:*algX*(S269A), pBBR1MCS-5:*algG*(D324A) and pBBR1MCS-5:*algX*(S269A):*algG*(D324A). These constructs were transferred into appropriate single- and double-gene knockout mutants via transconjugation using *E. coli* S17-1 as donor or electroporation. Resultant transformants were selected on PIA medium containing 300 μ g/mL gentamicin and confirmed by selecting cells with mucoid phenotypes followed by plasmid isolation and analysis. Phenotypic characterization of transformants included alginate isolation and quantification. All generated strains are listed in Table S1.

Chromosomal integration of *alg8-6his*, *alg44-6his*, *algG-6his* and *algX-6his* and *cis*-complementation of single-gene knockout mutants. In order to integrate genes encoding the respective hexahistidine (6his) tagged alginate protein into the genome, the plasmid mini-CTX-*lacZ* (53) was used and plasmids mini-CTX:*Palg8-6his*, mini-CTX:*Palg44-6his*, mini-CTX:*PalgG-6his* and mini-CTX:*PalgX-6his* were constructed as follows. The promoter region at -901 bp relative to the *algU* open reading frame was amplified using primers *palgUPstIF* and *palgUHindIII*R (54). The *alg8*, *alg44*, *algG* and *algX* regions were amplified and PCR products were ligated into pGEM-T Easy vector for sequence verification. The promoter region was hydrolyzed with *PstI* and *HindIII* and the genes were digested with *HindIII* and *BamHI* followed by ligation of fragments into mini-CTX-*lacZ* hydrolyzed with *PstI* and *BamHI*, resulting in the generation of abovementioned plasmids. These plasmids each were electroporated into PDO300 Δ *alg8*, PDO300 Δ *alg44*, PDO300 Δ *algG* and PDO300 Δ *algX*. Transformants were selected on PIA containing 150 μ g/mL tetracycline. Integration of promoter region and the genes into the genome was confirmed using PCR with primers *PserUp* and *PserDown*. To remove the mini-CTX-*lacZ* backbone plasmid pFLP2 was used as described above.

Site-specific mutations and deletions of *alg44* and *alg8*. Two highly conserved R residues of PilZ_{Alg44} domain's R17XXXR21 motif binding to secondary messenger c-di-GMP and the residues E322, H323 and E326 of Alg8 were mutated to D or A using either utilizing the QuikChange[®] II Site-Directed Mutagenesis Kit (Stratagene) or by DNA synthesis (GenScript). The resultant plasmids were pBBR1MCS-5:*alg44*(R17A), pBBR1MCS-5:*alg44*(R21A), pBBR1MCS-5:*alg44*(R21D)-6his, pBBR1MCS-5:*alg44*(R17A, R21A), pBBR1MCS-5:*alg8*(E322A), pBBR1MCS-5:*alg8*(H323A) and pBBR1MCS-5:*alg8*(E326A), pBBR1MCS-5:*alg44*(R17A):*alg8*(E322A), pBBR1MCS-5:*alg44*(R17A):*alg8*(H323A), pBBR1MCS-5:*alg44*(R17A):*alg8*(E326A), pBBR1MCS-5:*alg44*(R21A):*alg8*(E322A), pBBR1MCS-5:*alg44*(R21A):*alg8*(H323A), pBBR1MCS-5:*alg44*(R21A):*alg8*(E326A). Combinations of these mutated genes with *rocR* (PA3947) were also generated as mentioned in Table S1. Oligonucleotide deletion of PilZ_{Alg44} domain from amino acid 40 to 74 designated as (Δ 40-74aa_{PilZ}) and C-terminal truncation of a periplasmic part of Alg44 of 26 amino acids (Δ 364-389aa) were performed through the replacement of short synthesized DNA fragments containing these deletions yielding pBBR1MCS-5:*alg44-6his*(Δ 40-74aa_{PilZ}) and pBBR1MCS-5:*alg44-6his*(Δ 364-389aa). These plasmids were electroporated into PDO300 Δ *alg8*, PDO300 Δ *alg44* or PDO300 Δ *alg8* Δ *alg44* mutants generating PDO300 Δ *alg44* (pBBR1MCS-5:*alg44*(R21D)-6his), PDO300 Δ *alg44*(pBBR1MCS-5:*alg44-6his*(Δ 40-74aa_{PilZ})), PDO300 Δ *alg44*(pBBR1MCS-5:*alg44-6his*(Δ 364-389aa)), PDO300 Δ *alg44* (pBBR1MCS-5:*alg44*(R17A)), PDO300 Δ *alg44* (pBBR1MCS-5:*alg44*(R21A)), PDO300 Δ *alg8* (pBBR1MCS-5:*alg44*(E322A)), PDO300 Δ *alg8* (pBBR1MCS-5:*alg44*(H323A)), PDO300 Δ *alg8* (pBBR1MCS-5:*alg44*(E326A)), PDO300 Δ *alg8* Δ *alg44* (pBBR1MCS-5:*alg44*(R17A):*alg8*(E322A)), PDO300 Δ *alg8* Δ *alg44* (pBBR1MCS-5:*alg44*(R17A):*alg8*(H323A)), PDO300 Δ *alg8* Δ *alg44* (pBBR1MCS-5:*alg44*(R17A):*alg8*(E326A)), PDO300 Δ *alg8* Δ *alg44* (pBBR1MCS-5:*alg44*(R21A):*alg8*(E322A)), PDO300 Δ *alg8* Δ *alg44* (pBBR1MCS-5:*alg44*(R21A):*alg8*(H323A)), PDO300 Δ *alg8* Δ *alg44* (pBBR1MCS-5:*alg44*(R21A):*alg8*(E326A)).

5:*alg44*(R21A):*alg8*(H323A)), PDO300 Δ *alg8* Δ *alg44* (pBBR1MCS-5:*alg44*(R21A):*alg8*(E326A)). Transformants were selected on PIA medium supplemented by 300 μ g/mL gentamicin and confirmed by plasmid isolation and analysis.

***In vivo* detection of protein-protein interaction network.** Dependent on the applicability and the efficiency of protein-protein interaction methods for membrane-anchored proteins and those involved in the multi-protein complexes, three different methods including pull-down under native condition, *in vivo* chemical crosslinking and bacterial two-hybrid system (BACTH) were successfully applied. However different characteristics of proteins involved in alginate multi-protein complex were considered in designing these experiments and they are described as follows.

His-pull down under native condition. For pulling down hexahistidine-tagged Alg44 (Alg44-6his), Alg8 (Alg8-6his) and defective variants of Alg44-6his under native condition, a His-spin protein miniprep kit (Zymo Research) was used. Cells grown on solid media were scraped-off and washed twice with saline solution and pelleted. Enzymatic cell lysis was carried out by adding lysis buffer prepared with buffer A (100 mM NaH₂PO₄, 100 mM KCl, 10 mM Tris-HCl (pH 8.0), 1.5% Triton, Roche complete protease inhibitor EDTA-free) containing 0.1 mg/mL lysozyme and 0.1 mg/mL DNaseI and incubated on ice for 30 min and subsequently lysed by sonication. Cell debris was removed by centrifugation at 15,000 \times g for 20 min at 4 °C. Subsequently, ultracentrifugation at 100,000 \times g was carried out for 1 h at 4 °C to isolate the envelope fraction and embedded proteins. Sediments were solubilized with buffer A containing 10 mM imidazole and mixed with the resin. Buffer A supplemented with 50 mM and 400 mM imidazole was respectively used for washing twice and elution. Eluates were used for protein analysis.

***In vivo* chemical crosslinking.** For Alg44-6his proteins *in vivo* chemical crosslinking was performed using 400 mL overnight liquid cultures as described previously (20). Briefly, disuccinimidyl glutarate (DSG, Pierce) was used for covalently linking primary amine moieties of two lysine residues in the vicinity of 7.7Å. Crosslinking reaction was carried out in 5 mL of phosphate-buffered saline (PBS) containing cells and 1.5 mM DSG (dissolved in dimethyl sulfoxide (DMSO)) at 37 °C for 30 min and terminated with 20 mM Tris-HCl (f. conc., pH 7.5) for 15 min. Pelleted cells were enzymatically lysed with lysis buffer prepared with buffer B (150 mM NaCl, 100 mM Tris-HCl (pH 7.8), 0.2% Triton X-100, Roche complete protease inhibitor EDTA-free) containing 1 mg/mL lysozyme and 1 mg/mL DNaseI and incubated on ice for 20 min followed by sonication. Cell debris were removed using centrifugation at 15,000 \times g for 20 min and supernatants were centrifuged at 100,000 \times g for 1 h at 4 °C to isolate envelope fraction. Sediments were solubilized with protein-denaturing buffer C (8 M urea, 100 mM Tris-HCl (pH 8.0), 1 M NaCl, 1% Triton X-100, 0.2% *N*-lauroyl sarcosine, 10 mM imidazole). His-pull down

assay under denaturing condition was similar to abovementioned procedure except for using buffer C instead of buffer A in washing and eluting steps.

Bacterial two-hybrid assay. The adenylate cyclase-based two-hybrid kit (Euromedex) was employed to examine Alg8 and Alg44 interaction in a heterologous host. This experiment was designed to have a free signal peptide at N-terminal part of Alg8 and Alg44 and in a combinational manner in terms of low (pKNT25) or high (pUT18) copy number of plasmids containing the respective genes. Therefore, relevant genes were inserted at 5' end of coding region of T25 and T18 fragments of adenylate cyclase on plasmids pKNT25 and pUT18 producing plasmids pKNT25:*alg8*, pKNT25:*alg44*, pUT18:*alg8*, pUT18:*alg44*. After co-transformation of *E. coli* BTH101 competent cells with two plasmids, cells were plated on LB-X-gal-(5-bromo-4-chloro-3-indolyl- β -D-galactopyranoside, 20 mg/mL)-IPTG (0.5 mM) and incubated at 37°C for 48 h. Protein-protein interactions leading to functional adenylate cyclase activity were indicated by β -galactosidase activity in cell extracts of co-transformants grown in liquid culture as described (55). A level of β -galactosidase activity of at least 4-fold higher than that measured for BTH101 cells with pKNT25 and pUT18 (60-100 U/mg) or background was considered to indicate a protein-protein interaction. Each value was represented as the mean value \pm SD from five independent experiments. Negative controls were those transformants harboring plasmids with the respective hybrid genes each together with a plain vector. The plasmids expressing leucine-zipper domains included to the kit were used as positive control.

Isolation of cytoplasmic membrane. To confirm the localization of Alg8 and Alg44 in the cytoplasmic membrane of *E. coli* BTH101, the cytoplasmic membrane fraction was isolated as described previously with some modifications (56). Overnight culture of BTH101 transformants with pBBR1MCS-5:*alg8*-6his and pBBR1MCS-5:*alg44*-6his and empty pBBR1MCS-5 in addition to *P. aeruginosa* PDO300 Δ *alg8*(pBBR1MCS-5), PDO300 Δ *alg44*(pBBR1MCS-5) (as negative controls) and PDO300 Δ *alg8*(pBBR1MCS-5:*alg8*-6his), PDO300 Δ *alg44*(pBBR1MCS5:*alg44*-6his) (as positive controls) were subcultured in 1.5 liters of LB media. Cells were harvested by centrifugation at $7,000 \times g$ and 4 °C for 20 min. Tris-HCl (pH 8.3) was used for twice washing and sediments were subjected to enzymatic lysis by suspending in 20 mL of 20% sucrose in 30 mM Tris-HCl (pH 8.3), 1 mg/mL DNase I, 1 mg/mL RNase A, 1 mg/mL lysozyme and Roche complete protease inhibitor EDTA-free on ice for 20 min which was followed by sonication. Cell debris were removed and supernatants were then layered onto a sucrose density gradient containing 3 mL of 70% (wt/vol) and 3 mL of 52% (wt/vol) sucrose in Tris and centrifuged at $211,000 \times g$ for 3 h at 4 °C. The buoyant layers on top of 52% sucrose step were separated for protein analysis using SDS-PAGE (8% acrylamide gels) and immunoblotting utilizing anti-6his tag antibody as will be explained in protein detection section.

Assessment of the stability of Alg44 variants in the presence and absence of MucR (DGC/PDE)/rocR (PDE). Previously generated mutants including PDO300 Δ *mucR*, PDO300 Δ *mucR* (pBBR1MCS-5:*mucR*), PDO300 (pBBR1MCS-5:*rocR*), PDO300 Δ *mucR* (pBBR1MCS-5:*rocR*) were shown to be positively or negatively regulate alginate production through c-di-GMP synthesis (by MucR) or degradation (by RocR) (23). Also to use presumably nonfunctional Alg44 in binding to c-di-GMP and/or in alginate polymerization (8, 25), the mutants PDO300 Δ *alg44* (pBBR1MCS-5:*alg44*(R21D)-6his), PDO300 Δ *alg44*(pBBR1MCS-5:*alg44*-6his(Δ 40-74aa_{PIIZ})) and PDO300 Δ *alg44*(pBBR1MCS-5:*alg44*-6his(Δ 364-389aa)) were generated. Using these mutants we examined direct effect of c-di-GMP and defective variants of Alg44 on its localization and stability in planktonic and biofilm cells. Cells grown on solid media or in liquid cultures as described above were washed twice with saline. Enzymatic cell lysis was performed using abovementioned lysis buffer prepared in buffer A followed by sonication and isolation of cell envelope fraction by ultracentrifugation at 100,000 \times g for 1 h at 4 °C. Pellets were solubilized with buffer A for protein analysis.

Protein analysis. Protein samples were generally analyzed utilizing SDS-PAGE (8% acrylamide gels). For analyzing chemically crosslinked proteins, 4-15% Mini-Protean TGX precast gradient gels (Bio-Rad) were used. Immunoblotting by using an iBlot dry-blotting system (Invitrogen) was employed to detect proteins as described previously (20) in which the antibodies anti-Alg44 (1:10,000), anti-AlgK (1:10,000), anti-AlgG (1:10,000), anti-AlgX (1:7,000), or anti-AlgE (1:5,000) in 2% skim milk and anti-Alg8 (1.5:5,000) in 2% bovine serum albumin-fraction V (Gibco/Invitrogen) were used. Treatment of membrane with commercial secondary antibody, anti-IgG anti-rabbit antibodies labeled with horseradish peroxidase (HRP) (Abcam), followed by resolving with SuperSignal West Pico chemiluminescent substrate (Thermoscientific) were carried out and the resulting membranes were developed on X-ray film (Kodak, Rochester). For the detection of hexahistidine-tagged proteins, a HisProbe-HRP kit (Thermoscientific) was used according to the manufacturer's instruction.

Alginate purification and quantification. A total of 2 mL of bacterial overnight cultures grown in LB medium supplemented with appropriate antibiotic were harvested and washed twice with saline solution. Then, the harvested cell sediments were re-suspended in 1 mL of saline solution and 200 μ L of cell suspension was plated onto each PIA medium (with three repetitions) containing 300 μ g/mL of gentamicin and incubated at 37 °C for 72 h. Cells of each plate were scraped off and suspended in saline solution until all alginate materials were completely dissolved. To separate cells from alginate-containing supernatant, the suspensions were pelleted and alginates in supernatants were precipitated with equal volume of ice-cold isopropanol. Additionally, cellular sediments were freeze-dried and the final weights were determined. The alginate precipitants were freeze-dried and then re-dissolved in 50 mM Tris-HCl pH 7.4, 10 mM MgCl₂ to a final concentration of 0.5% (wt/vol), followed by incubation with 15 μ g/mL DNaseI and 15 μ g/mL RNaseI at 37 °C for 6 h. Then, Pronase E was added to a final concentration of 20

$\mu\text{g/mL}$ and incubated for further 18 h at 37 °C. Alginate solutions were dialyzed (12-14 kDa MWCO, ZelluTrans/Roth mini dialyzer, Carl Roth GmbH & Co) against 5 L of ultrapure H₂O for 48 h. Finally, alginates were precipitated with equal volume of ice-cold isopropanol and freeze-dried for uronic acid assay and biochemical analysis.

Following a modified protocol for alginate quantification or uronic acid assay (9) and using purified alginic acid from brown algae (Sigma-Aldrich) as a standard, alginate samples were dissolved in 200 μL of ultrapure water at concentrations between 0.25 and 0.05 mg/mL. Each sample was mixed with 1.2 mL of tetraborate solution (0.0125 M disodium tetraborate in concentrated sulfuric acid) and incubated on ice for 10 min followed by incubation at 100°C for 5 min and then cooled down on ice for further 5 min. By adding 20 μL of 3-phenylphenol reagent (0.15% of 3-phenylphenol in 0.125 M NaOH), reactions were developed within 1 min of vortexing. For each sample and dilution a negative control was assayed by using 0.125 M NaOH instead of the 3-phenylphenol reagent. Uronic acid concentrations were determined spectrophotometrically at a wavelength of 520 nm.

Size exclusion chromatography-multiangle laser light scattering (SEC-MALLS) analysis.

Polymerization degree of alginates were analyzed by determining the average molecular weights of the alginates by employing SEC-MALLS (Waters 2690 Alliance separations module; Waters 450 variable wavelength detector set at 280 nm; DAWN-EOS multi-angle laser light scattering detector with a laser at 690 nm (Wyatt Technology Corp., Santa Barbara, CA, USA); Waters 2410 refractive index monitor). Purified samples were dissolved in 0.1 M NaNO₃ (2 mg/mL) and allowed to be fully hydrated by incubating at room temperature overnight. Immediately prior to analysis, samples were pre-heated at 80 °C for 5 min and injected (100 μL) and eluted with 0.1 M NaNO₃ (0.7 mL/min, 60 °C) from two columns (TSK-Gel G5000P_{WXL} and G4000P_{WXL}, 300 \times 7.8 mm, Tosoh Corp.) connected in series. ASTRA software (version 6.1.1.17, Wyatt Technology Corp.) and dn/dc of 0.150 mL/g was used for determining weight-average molecular weights (\overline{M}_w) and number-average molecular weights (\overline{M}_n) and polydispersity index (PI) via the fraction $\overline{M}_w/\overline{M}_n$. In the case of a perfectly monodisperse (homogeneous) polymer PI value equals 1.0.

¹H-nuclear magnetic resonance (NMR) spectroscopy analysis. Compositional analysis of alginate samples was done by using ¹H-NMR. The spectra were recorded at 90 °C with a JEOL 270 NMR spectrometer (6.34 T) operating at 270 MHz for proton. Samples were prepared as described by Grasdalen et al (57). The chemical shifts were expressed in ppm downfield from the signal for 3-(trimethylsilyl) propanesulfonate. The integration of the ¹H-NMR signals allowed us to determine the composition of the different deacetylated alginate samples and their acetylation degree (58-60). For alkaline deacetylation 30 mL of 1% alginates in saline solution were treated with 12 mL of 1M NaOH in 65 °C for 30 min and neutralized with 12 mL of 1M HCl. Treated samples were then dialyzed against 5 L of distilled water for 48 h and then freeze-dried.

Fourier Transform Infrared Spectrometry (FTIR) analysis. This analysis was employed to confirm the acetylation of the alginate samples and the spectra were recorded as KBr discs with a Nicolet 5700 FTIR spectrometer in the range of 400–4000 cm^{-1} . FTIR band associated with *o*-acetyl groups of the alginate were observed at 1,730 and 1,250 cm^{-1} (30, 61).

Microrheological analysis. In order to measure viscoelastic property of the alginates, the mean-square displacement (MSD) of probe particles embedded in the samples and in turn the viscoelastic moduli (G' (elastic) and G'' (viscose)) were measured (62-64). A 2.8 μL aliquot of a 2.5% (wt/vol) suspension of Polybead® polystyrene microspheres (0.5 μm) (Polysciences) was mixed with 250 μL aliquot of 0.1% alginate samples in Milli-Q water. Particle motion was recorded using an inverted microscope (Nikon Eclipse TE2000-U) on an air damped table (Photon Control) equipped with an Andor Neo CMOS camera operated at 204 fps, and a 60x 1.2 NA (Nikon, Plan Apo VC 60x WI) water immersion objective lens. Image series acquired for approximately four seconds and x-y coordinate data extracted using polyparticle tracking software (65). An in-house program was used to calculate the MSD with a program to extract the rheological information (66).

Continuous-culture flow cell biofilms and quantitative analysis. Biofilm architecture analysis was performed for those mutants producing alginates with very distinct composition and properties from each other including PDO300(pBBR1MCS-5), PDO300 Δ alg8(pBBR1MCS-5:alg8), PDO300 Δ alg44(pBBR1MCS-5:alg44), PDO300 Δ algG(pBBR1MCS-5:algG), PDO300 Δ algG(pBBR1MCS-5:algG(D324A)), PDO300 Δ algX(pBBR1MCS-5:algX), PDO300 Δ algX(pBBR1MCS-5:algX(S269A)) and PDO300 Δ algX Δ algG(pBBR1MCS-5:algX(S269A):algG(D324A)). Each mutant was grown in continuous-culture flow cells (channel dimensions of 4 mm by 40 mm by 1.5 mm) at 37 °C (67). A 500 μL suspension of cells at early-stationary-phase was injected into each channel and kept upside down for 4 hours. Then, flow was started with a mean flow of 0.3 mL/min, corresponding to a laminar flow with a Reynolds number of 5 (23, 68). The flow cells were then incubated at 37 °C for 24 h. Biofilms were stained utilizing the LIVE/DEAD BacLight bacterial viability kit (Molecular Probes) and visualized using confocal laser scanning microscopy (Leica SP5 DM6000B). For quantitative analysis of biofilms IMARIS image analysis software (Bitplane) was employed. Biofilm architecture and appearance, biovolume (μm^3), the ratio of biovolume per unit area ($\mu\text{m}^3/\mu\text{m}^2$), dead-to-live ratio, compactness and thickness of base layers were analyzed (68-70).

Motility assay. Motilities including twitching, swarming and swimming were assessed by the method explained by Pang et al (44) with modification. The medium consisted of modified M9 medium (20 mM NH_4Cl ; 12 mM Na_2HPO_4 ; 8.6 mM NaCl ; 1 mM MgSO_4 ; 1 mM $\text{CaCl}_2 \cdot 2\text{H}_2\text{O}$; and 10 mM dextrose, supplemented with 0.5% (wt/vol) Casamino acids (Difco) (23) solidified with 1% , 0.5% and 0.3% (wt/vol) Bacto agar (Difco) respectively for twitching, swarming and swimming assays. Petri dishes were kept under laminar flow for 60 min and then swarming and

swimming plates were immediately inoculated with 5µL of stationary-phase bacterial culture while for twitching stab-inoculation to the underlying petri dishes was performed using sterile toothpicks. Plates were incubated at 30 °C for 18-24 h. Swarming and swimming were assessed by measuring colony diameters and twitching zone was measured up after removing agar layer, washing free cells and staining with 1% crystal violet. All experiments were done in triplicates.

ACKNOWLEDGMENTS. We are thankful to Lynne Howell from the University of Toronto and Dennis E. Ohman from Virginia Commonwealth University for providing antibodies and Iain D. Hay for advice and technical assistance, Manawatu Microscopy and Imaging Centre (MMIC) of Massey University and especially Matthew Savoian for microscopic technical assistance and Martin A. K. Williams and Bradley W. Mansel assisting us for microrheology analysis. This work was supported by grants from Massey University Research Fund and the MacDiarmid Institute of Advanced Materials and Nanotechnology (New Zealand) to B.H.A.R. M.F.M is funded by a Massey University Doctoral scholarship.

References

1. Rehm BH, Grabert E, Hein J, & Winkler UK (1994) Antibody response of rabbits and cystic fibrosis patients to an alginate-specific outer membrane protein of a mucoid strain of *Pseudomonas aeruginosa*. *Microbial pathogenesis* 16(1):43-51.
2. Pedersen SS, Hoiby N, Espersen F, & Koch C (1992) Role of alginate in infection with mucoid *Pseudomonas aeruginosa* in cystic fibrosis. *Thorax* 47(1):6-13.
3. Hay I, Rehman, Z., Ghafoor, A., and Rehm, B. (2010) Bacterial biosynthesis of alginates. *Journal of Chemical Technology and Biotechnology* 85(6):752-759.4. Hay ID, Ur Rehman Z, Moradali MF, Wang Y, & Rehm BH (2013) Microbial alginate production, modification and its applications. *Microb Biotechnol* 6(6):637-650.
5. Franklin MJ, Nivens DE, Weadge JT, & Howell PL (2011) Biosynthesis of the *Pseudomonas aeruginosa* Extracellular Polysaccharides, Alginate, Pel, and Psl. *Front Microbiol* 2:167.
6. Chitnis CE & Ohman DE (1993) Genetic analysis of the alginate biosynthetic gene cluster of *Pseudomonas aeruginosa* shows evidence of an operonic structure. *Molecular microbiology* 8(3):583-593.
7. Rehm BHA, Remminghorst U, & Hay ID (2009) Molecular characterization of Alg8, a putative glycosyltransferase, involved in alginate polymerization. *Journal of Biotechnology* 140(3-4):176-183.
8. Lory S, Merighi M, Lee VT, Hyodo M, & Hayakawa Y (2007) The second messenger bis-(3'-5')-cyclic-GMP and its PilZ domain-containing receptor Alg44 are required for alginate biosynthesis in *Pseudomonas aeruginosa*. *Molecular Microbiology* 65(4):876-895.
9. Rehm BHA & Remminghorst U (2006) In vitro alginate polymerization and the functional role of Alg8 in alginate production by *Pseudomonas aeruginosa*. *Applied and Environmental Microbiology* 72(1):298-305.
10. Rehm BHA, Hay ID, & Remminghorst U (2009) MucR, a Novel Membrane-Associated Regulator of Alginate Biosynthesis in *Pseudomonas aeruginosa*. *Applied and Environmental Microbiology* 75(4):1110-1120.
11. Baker P, *et al.* (2014) *P. aeruginosa* SGNH Hydrolase-Like Proteins AlgJ and AlgX Have Similar Topology but Separate and Distinct Roles in Alginate Acetylation. *PLoS Pathog* 10(8):e1004334.

12. Franklin MJ & Ohman DE (2002) Mutant analysis and cellular localization of the AlgI, AlgJ, and AlgF proteins required for O acetylation of alginate in *Pseudomonas aeruginosa*. *J Bacteriol* 184(11):3000-3007.
13. Riley LM, *et al.* (2013) Structural and functional characterization of *Pseudomonas aeruginosa* AlgX: role of AlgX in alginate acetylation. *J Biol Chem*.
14. Jain S, Franklin MJ, Ertesvag H, Valla S, & Ohman DE (2003) The dual roles of AlgG in C-5-epimerization and secretion of alginate polymers in *Pseudomonas aeruginosa*. *Mol Microbiol* 47(4):1123-1133.
15. Schiller NL, Robles-Price A, Wong TY, Sletta H, & Valla S (2004) AlgX is a periplasmic protein required for alginate biosynthesis in *Pseudomonas aeruginosa*. *Journal of Bacteriology* 186(21):7369-7377.
16. Bakkevig K, *et al.* (2005) Role of the *Pseudomonas fluorescens* alginate lyase (AlgL) in clearing the periplasm of alginates not exported to the extracellular environment. *J Bacteriol* 187(24):8375-8384.
17. Keiski CL, *et al.* (2010) AlgK is a TPR-containing protein and the periplasmic component of a novel exopolysaccharide secretin. *Structure* 18(2):265-273.
18. Rehman ZU & Rehm BH (2013) Dual roles of *Pseudomonas aeruginosa* AlgE in secretion of the virulence factor alginate and formation of the secretion complex. *Appl Environ Microbiol* 79(6):2002-2011.
19. Albrecht MT & Schiller NL (2005) Alginate lyase (AlgL) activity is required for alginate biosynthesis in *Pseudomonas aeruginosa*. *J Bacteriol* 187(11):3869-3872.
20. Rehman ZU, Wang Y, Moradali MF, Hay ID, & Rehm BH (2013) Insights into the assembly of the alginate biosynthesis machinery in *Pseudomonas aeruginosa*. *Appl Environ Microbiol* 79(10):3264-3272.
21. Hay ID, Schmidt O, Filitcheva J, & Rehm BH (2011) Identification of a periplasmic AlgK-AlgX-MucD multiprotein complex in *Pseudomonas aeruginosa* involved in biosynthesis and regulation of alginate. *Appl Microbiol Biotechnol* 93(1):215-227.
22. Kulasakara H, *et al.* (2006) Analysis of *Pseudomonas aeruginosa* diguanylate cyclases and phosphodiesterases reveals a role for bis-(3'-5')-cyclic-GMP in virulence. *Proc Natl Acad Sci U S A* 103(8):2839-2844.
23. Hay ID, Remminghorst U, & Rehm BH (2009) MucR, a novel membrane-associated regulator of alginate biosynthesis in *Pseudomonas aeruginosa*. *Appl Environ Microbiol* 75(4):1110-1120.
24. Rehm BHA & Remminghorst U (2006) Alg44, a unique protein required for alginate biosynthesis in *Pseudomonas aeruginosa*. *FEBS Letters* 580(16):3883-3888.
25. Ohman DE, Oglesby LL, & Jain S (2008) Membrane topology and roles of *Pseudomonas aeruginosa* Alg8 and Alg44 in alginate polymerization. *Microbiology-Sgm* 154:1605-1615.
26. Steiner S, Lori C, Boehm A, & Jenal U (Allosteric activation of exopolysaccharide synthesis through cyclic di-GMP-stimulated protein-protein interaction. *EMBO J* 32(3):354-368.
27. Rehm B (2009) *Microbial production of biopolymers and polymer precursors : applications and perspectives* (Caister Academic, Wymondham) pp viii, 293 p., [291] p. of plates.
28. Morgan JL, Strumillo J, & Zimmer J (2013) Crystallographic snapshot of cellulose synthesis and membrane translocation. *Nature* 493(7431):181-186.
29. Kelley LA & Sternberg MJ (2009) Protein structure prediction on the Web: a case study using the Phyre server. *Nat Protoc* 4(3):363-371.
30. Franklin MJ & Ohman DE (1993) Identification of algF in the alginate biosynthetic gene cluster of *Pseudomonas aeruginosa* which is required for alginate acetylation. *J Bacteriol* 175(16):5057-5065.
31. Franklin MJ & Ohman DE (1996) Identification of algI and algJ in the *Pseudomonas aeruginosa* alginate biosynthetic gene cluster which are required for alginate O acetylation. *J Bacteriol* 178(8):2186-2195.

32. Franklin MJ, *et al.* (1994) Pseudomonas aeruginosa AlgG is a polymer level alginate C5-mannuronan epimerase. *J Bacteriol* 176(7):1821-1830.
33. Wolfram F, *et al.* (2014) Catalytic mechanism and mode of action of the periplasmic alginate epimerase AlgG. *J Biol Chem* 289(9):6006-6019.
34. Ma L, *et al.* (2009) Assembly and development of the Pseudomonas aeruginosa biofilm matrix. *PLoS Pathog* 5(3):e1000354.
35. Billings N, *et al.* (2013) The extracellular matrix Component Psl provides fast-acting antibiotic defense in Pseudomonas aeruginosa biofilms. *PLoS Pathog* 9(8):e1003526.
36. Rehm B (2009) *Alginates : biology and applications* (Springer, Dordrecht ; New York) pp viii, 266 p.
37. Akama H, *et al.* (2004) Crystal structure of the membrane fusion protein, MexA, of the multidrug transporter in Pseudomonas aeruginosa. *J Biol Chem* 279(25):25939-25942.
38. Morona R, Purins L, Tocilj A, Matte A, & Cygler M (2009) Sequence-structure relationships in polysaccharide co-polymerase (PCP) proteins. *Trends Biochem Sci* 34(2):78-84.
39. Morona R, Van Den Bosch L, & Daniels C (2000) Evaluation of Wzz/MPA1/MPA2 proteins based on the presence of coiled-coil regions. *Microbiology* 146 (Pt 1):1-4.
40. Carter JA, *et al.* (2009) The cellular level of O-antigen polymerase Wzy determines chain length regulation by WzzB and WzzpHS-2 in Shigella flexneri 2a. *Microbiology* 155(Pt 10):3260-3269.
41. Morgan JL, McNamara JT, & Zimmer J (2014) Mechanism of activation of bacterial cellulose synthase by cyclic di-GMP. *Nat Struct Mol Biol* 21(5):489-496.
42. Schurks N, Wingender J, Flemming HC, & Mayer C (2002) Monomer composition and sequence of alginates from Pseudomonas aeruginosa. *Int J Biol Macromol* 30(2):105-111.
43. Galindo E, Pena C, Nunez C, Segura D, & Espin G (2007) Molecular and bioengineering strategies to improve alginate and polyhydroxyalkanoate production by Azotobacter vinelandii. *Microb Cell Fact* 6:7.
44. Pang CM, Hong P, Guo H, & Liu WT (2005) Biofilm formation characteristics of bacterial isolates retrieved from a reverse osmosis membrane. *Environ Sci Technol* 39(19):7541-7550.
45. Hengge R (2009) Principles of c-di-GMP signalling in bacteria. *Nat Rev Microbiol* 7(4):263-273.
46. Simm R, Morr M, Kader A, Nimtz M, & Romling U (2004) GGDEF and EAL domains inversely regulate cyclic di-GMP levels and transition from sessility to motility. *Mol Microbiol* 53(4):1123-1134.
47. Chin KH, *et al.* (2012) Structural polymorphism of c-di-GMP bound to an EAL domain and in complex with a type II PilZ-domain protein. *Acta Crystallogr D Biol Crystallogr* 68(Pt 10):1380-1392.
48. Tielen P, Strathmann M, Jaeger KE, Flemming HC, & Wingender J (2005) Alginate acetylation influences initial surface colonization by mucoid Pseudomonas aeruginosa. *Microbiol Res* 160(2):165-176.
49. Gloag ES, *et al.* (2013) Stigmergy: A key driver of self-organization in bacterial biofilms. *Commun Integr Biol* 6(6):e27331.
50. Schlegel HG, Kaltwasser H, & Gottschalk G (1961) [A submersion method for culture of hydrogen-oxidizing bacteria: growth physiological studies]. *Arch Mikrobiol* 38:209-222.
51. Hoang TT, Karkhoff-Schweizer RR, Kutchma AJ, & Schweizer HP (1998) A broad-host-range Flp-FRT recombination system for site-specific excision of chromosomally-located DNA sequences: application for isolation of unmarked Pseudomonas aeruginosa mutants. *Gene* 212(1):77-86.
52. Kovach ME, *et al.* (1995) Four new derivatives of the broad-host-range cloning vector pBBR1MCS, carrying different antibiotic-resistance cassettes. *Gene* 166(1):175-176.
53. Schweizer HP & Chuanchuen R (2001) Small broad-host-range lacZ operon fusion vector with low background activity. *Biotechniques* 31(6):1258, 1260, 1262.

54. Schurr MJ, Yu H, Boucher JC, Hibler NS, & Deretic V (1995) Multiple promoters and induction by heat shock of the gene encoding the alternative sigma factor AlgU (sigma E) which controls mucoidy in cystic fibrosis isolates of *Pseudomonas aeruginosa*. *J Bacteriol* 177(19):5670-5679.
55. Karimova G, Dautin N, & Ladant D (2005) Interaction network among *Escherichia coli* membrane proteins involved in cell division as revealed by bacterial two-hybrid analysis. *Journal of Bacteriology* 187(7):2233-2243.
56. Hancock RE & Nikaido H (1978) Outer membranes of gram-negative bacteria. XIX. Isolation from *Pseudomonas aeruginosa* PAO1 and use in reconstitution and definition of the permeability barrier. *J Bacteriol* 136(1):381-390.
57. Grasdalen H, Larsen B, & Smidsrod O (1979) Pmr Study of the Composition and Sequence of Uronate Residues in Alginates. *Carbohydrate Research* 68(1):23-31.
58. Donati IP, S. (2009) Material Properties of Alginates in *Alginates; Biology and Applications*; Rhem, B. H. A. Ed.; Springer-Verlag; Berlin Heidelberg.1-53.
59. Skjak-Braek G, Grasdalen H, & Larsen B (1986) Monomer sequence and acetylation pattern in some bacterial alginates. *Carbohydr Res* 154:239-250.
60. Pawar SN & Edgar KJ (Chemical modification of alginates in organic solvent systems. *Biomacromolecules* 12(11):4095-4103.
61. Nivens DE, Ohman DE, Williams J, & Franklin MJ (2001) Role of alginate and its O acetylation in formation of *Pseudomonas aeruginosa* microcolonies and biofilms. *J Bacteriol* 183(3):1047-1057.
62. Williams MAK VR, Pinder DN, Hemar Y (2008) Microrheological studies offer insights into polysaccharide gels. *Journal of Non-Newtonian Fluid Mechanics* 149:63-70.
63. Hemar Y & Pinder DN (2006) DWS microrheology of a linear polysaccharide. *Biomacromolecules* 7(3):674-676.
64. Mansel BW; Keen SAJ PP, Hemar Y, Williams MAK (2013) A Practical Review of Microrheological Techniques. *Rheology - New Concepts, Applications and Methods*, Rajkumar Durairaj, InTech, Rijeka Croatia.
65. Rogers SS, Waigh TA, Zhao X, & Lu JR (2007) Precise particle tracking against a complicated background: polynomial fitting with Gaussian weight. *Phys Biol* 4(3):220-227.
66. Mason TG GK, van Zanten JH, Wirtz D, Kuo SC (1997) Particle Tracking Microrheology of Complex Fluids. *Physical Review Letters* 79:3282-3285.
67. Campisano A, Schroeder C, Schemionek M, Overhage J, & Rehm BH (2006) PsID is a secreted protein required for biofilm formation by *Pseudomonas aeruginosa*. *Appl Environ Microbiol* 72(4):3066-3068.
68. Ghafoor A, Hay ID, & Rehm BH (2011) Role of exopolysaccharides in *Pseudomonas aeruginosa* biofilm formation and architecture. *Appl Environ Microbiol* 77(15):5238-5246.
69. Kuehn M, *et al.* (1998) Automated confocal laser scanning microscopy and semiautomated image processing for analysis of biofilms. *Appl Environ Microbiol* 64(11):4115-4127.
70. Heydorn A, *et al.* (2000) Quantification of biofilm structures by the novel computer program COMSTAT. *Microbiology* 146 (Pt 10):2395-2407.

Table 1. Composition and molecular weight analyses of alginate produced by different mutants

Mutant		F _G	F _M	F _{GMMG}	F _{MM}	Ac. %	Mw (kDa)	Mn (kDa)	PI
1-	300 +MCS5	0.3	0.7	0.29	0.41	32	3927 (±0.864%)	3832 (±0.842%)	1.025 (±1.207%)
2-	300Δ8+ MCS5: <i>alg8</i>	0.18	0.82	0.17	0.65	11.3	3045 (±0.556%)	3037 (±0.551%)	1.003 (±0.783%)
3-	300Δ44+ MCS5: <i>alg44</i>	0.18	0.82	0.18	0.64	26.8	3831 (±0.963%)	3650 (±0.950%)	1.05 (±1.353%)
4-	300Δ44Δ8+ MCS5: <i>alg44;alg8</i>	0.17	0.83	0.17	0.66	11	3369 (±0.839%)	3352 (±0.821%)	1.005 (±1.173%)
5-	300ΔX+ MCS5: <i>algX</i>	0.36	0.64	0.36	0.28	9.8	2460 (±0.932%)	2447 (±0.913%)	1.005 (±1.304%)
6-	300ΔX+ MCS5: <i>algX(S269A)</i>	0.36	0.64	0.36	0.28	0	2086 (±0.960%)	2065 (±0.944%)	1.010 (±1.346%)
7-	300ΔG+ MCS5: <i>algG</i>	0.32	0.68	0.32	0.36	23.3	2755 (±1.041%)	2726 (±0.986%)	1.011 (±1.434%)
8-	300ΔG+ MCS5: <i>algG(D324A)</i>	0	1	0	1	25.2	4653 (±1.097%)	4575 (±1.117%)	1.017 (±1.566%)
9-	300ΔXΔG+ MCS5: <i>algX;algG</i>	0.34	0.66	0.34	0.32	28.4	3076 (±1.051%)	3044 (±1.029%)	1.011 (±1.471%)
10-	300ΔXΔG+ MCS5: <i>algX(S269A); algG(D324A)</i>	0	1	0	1	0	1811 (±0.884%)	1716 (±0.888%)	1.055 (±1.253%)
11-	300Δ44ΔG+ MCS5: <i>alg44+algG</i>	0.22	0.78	0.22	0.56	14.5	2907 (±0.966%)	2861 (±0.944%)	1.016 (±1.351%)

300:PDO300; MCS5: pBBR1MCS-5.

Table 2. Compactness and dead/live ratio calculated for analyzed biofilms

mutant	Compactness	Dead/live
300 Δ 8+MCS5: <i>alg8</i>	6.09E+02	1.43 \pm 0.10
300 Δ 44+ MCS5: <i>alg44</i>	4.43E+02	1.17 \pm 0.04
300 Δ G+ MCS5: <i>algG</i>	2.77E+02	0.70 \pm 0.06
300 Δ G+ MCS5: <i>algG</i> (D324A)	1.68E+02	0.97 \pm 0.04
300 Δ X+ MCS5: <i>algX</i>	3.00E+02	0.42 \pm 0.02
300 Δ X+ MCS5: <i>algX</i> (S269A)	2.20E+02	0.55 \pm 0.02
300 Δ G Δ X+MCS5: <i>algG</i> (D324A): <i>algX</i> (S269A)	1.20E+03	0.49 \pm 0.03
300+MCS5	4.46E+02	2.40 \pm 0.29
300 Δ 8+MCS5	1.39E+02	1.46
300 Δ 44+MCS5	1.42E+02	0.7
300 Δ G+MCS5	8.90E+01	1.01
300 Δ X+MCS5	1.16E+02	0.94

300:PDO300; MCS5: pBBR1MCS-5.

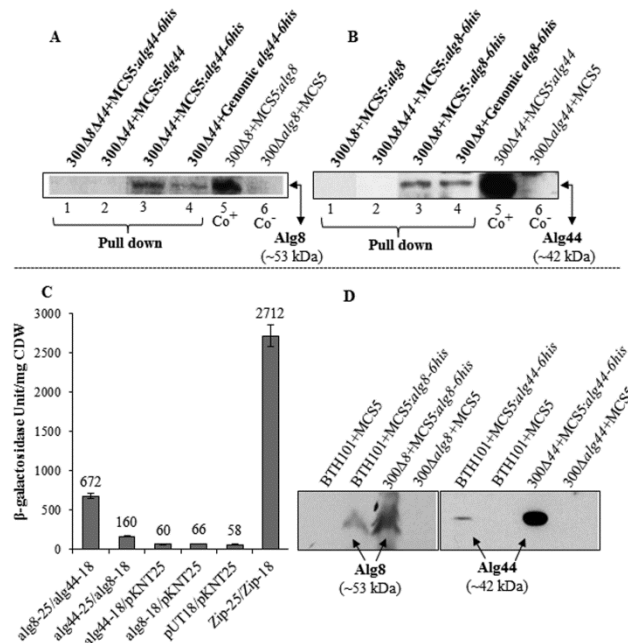


Figure 1. Alg8/Alg44 protein-protein interaction. His-tag based pull down assays (A, B) and bacterial two hybrid system analysis (C, D) show protein-protein interaction between Alg8 and Alg44. Envelope fractions of the cells grown on solid media were subjected to pull down assays under non-denaturing condition (lanes 1-4 in both blots). Immunoblots were developed using anti-Alg8 antibodies (A) and anti-Alg44 antibodies (B). Alg8 and Alg44 interaction was detected by respective co-purification of the non-His-tagged interacting protein partner from corresponding genes either integrated into the genome or localized on a plasmid (lane 3, 4 in both blots). Lanes 1 and 2 in both blots belong to negative controls whose native proteins (without his-tag) were present as single protein without the potentially interacting protein partner in a respective double knockout mutant background. (C) Bacterial two-hybrid analysis showed the *in vivo* interaction between Alg8 and Alg44 proteins by reconstitution of active adenylate cyclase in *E. coli*. The appropriate pUT18 and pKNT25 derivatives were co-transformed into the adenylate cyclase negative mutant *E. coli* BTH101 and the co-transformants were screened on LB medium containing 0.5 mM IPTG and 20 mg/ml X-gal after 48 hours incubation at 37 °C. The pUT18 and pKNT25 vectors were used as a negative control (background) in addition to transformants with one of the constructs and one empty vector, whilst the pUT18c-Zip and pKNT25-Zip plasmid-pair was used as a positive control. Fourfold β -galactosidase activity higher than background was regarded as indicator of interaction. This experiment was repeated 5-times independently for each transformant. The mean values plus the standard deviation were indicated. (D) Immunoblots show production and subcellular localization of Alg8 and Alg44 to cytoplasmic membrane of *E. coli* BTH101. PDO300 Δ alg8 and PDO300 Δ alg44 harboring empty plasmids were used as negative controls and *in trans* complemented ones with the plasmid harboring *alg8-6his* and *alg44-6his* were applied as positive controls. Anti-his tag antibodies were used to develop the immunoblots. The relevant part of the immunoblot was shown. 300: PDO300; 8, 44: Alg8, Alg44; MCS5: pBBR1MCS-5; Ab: antibody; Co+/-: positive/negative control; CDW: cellular dry weight; -18: pUT18; -25: pKNT25.

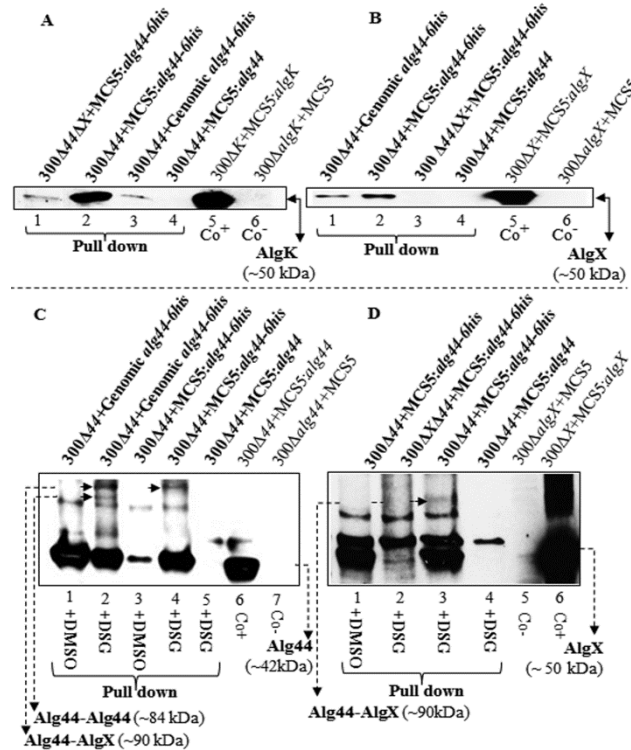


Figure 2. Protein-protein interaction analysis indicates interaction of Alg44-AlgK, Alg44-AlgX and Alg44-Alg44 (dimer). (A, B) His-tag based pull down assays show interactions of Alg44-AlgK and Alg44-AlgX. To detect Alg44-associated protein interaction network, envelope fractions of the cells (PDO300 Δ alg44(pBBR1MCS-5:alg44-6his) and PDO300 Δ alg44 with genomic alg44-6his) grown on solid media were solubilized with non-denaturing buffer and subjected to pull down assays under non-denaturing condition. Immunoblots were developed using anti-AlgK (A) or anti-AlgX (B) antibodies. (A) Immunoblot shows Alg44-AlgK interaction in both cases of *in trans* and *in cis* complementation of mutants with alg44-6his (lanes 2, 3). AlgK was pulled down using His-tagged Alg44 in the absence of AlgX in double-gene knockout mutant in alg44 and algX harboring MCS5:alg44-6his (lane 1). The elutes of complemented mutants producing non-his-tagged protein lacked AlgK (lane 4). (B) Immunoblot shows Alg44-AlgX interaction using pull-down analysis in the presence Alg44-6his produced either by *in trans* or *in cis* complementation (lanes 1, 2). This complex was not found in elutes of negative controls with native protein (without his-tag) or his-tagged Alg44 in relevant double-gene knockout mutant (lanes 3, 4). (C, D) Immunoblots demonstrate *in vivo* Alg44 dimerization and Alg44-AlgX interaction using chemical cross-linking. The mutants PDO300 Δ alg44 (pBBR1MCS-5:alg44-6his) and PDO300 Δ alg44 with genomic alg44-6his were applied and grown in liquid media. After crosslinking with DSG (7.7 Å) and extracting envelop fraction of cells, protein analysis was performed under denaturing conditions. Alg44 dimer band (~84 kDa) reacted only with Alg44 antibody (C, lane 2). Another band (~90 kDa) (lanes 2,4) which reacted with Alg44 and AlgX antibodies showing their interaction was previously reported from *in trans* complemented mutant with alg44-6his gene (blot D, lane 3) (1) but its detection in *in cis* complementation was new report in this study (blot C, lane 2). These bands were not detected in the eluents of mutants with native Alg44 with DSG and Alg44-6his treated with DMSO as negative controls (blot C, lanes 1,3; blot D, lanes 1, 4). 300: PDO300; MCS5: BBR1MCS-5; Ab: antibody; Co+/-: positive/negative control.

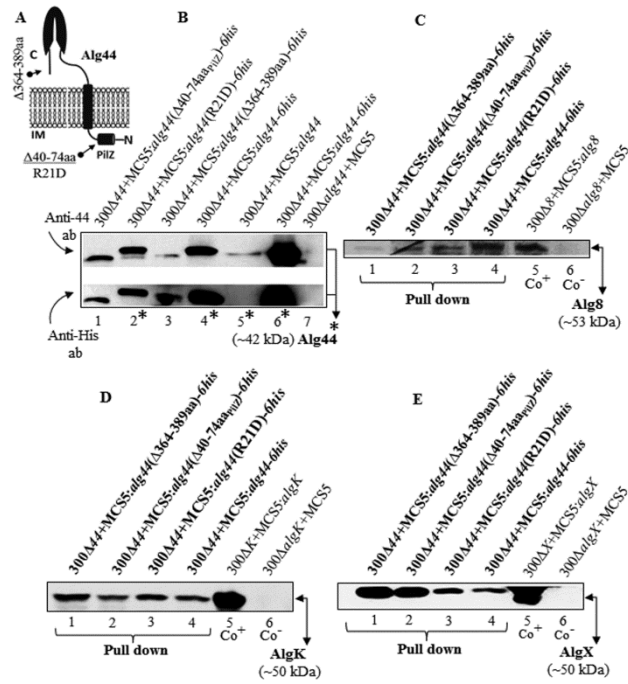


Figure3. Localization, stability and protein-protein interaction of Alg44 variants. (A) Schematic view of deleted or point-mutated region of Alg44. Immunoblots of envelope fraction showed that Alg44 with deletions and a site-specific mutation in the PilZ domain and a C-terminal deletion did not disrupt localization of Alg44 (immunoblot B, lanes 1-3). (B) Immunoblots were developed with anti-Alg44 antibody (upper blot) and anti-His tag antibody (lower blot). Lanes 4-7 represent negative and positives controls. (C-E) Immunoblots showed protein-protein interaction of Alg44 variants with Alg8, AlgK and AlgX by using pull-down experiments using His-tagged variants of Alg44. Immunoblots were developed using anti-Alg8 (C), anti-AlgK (D) and anti-AlgX (E) antibodies, respectively. Lanes 1-4 in each blot belong to His-pull down assays. 300: PDO300; MCS5: pBBR1MCS-5; Ab: antibody; Co+/-: positive/negative control.

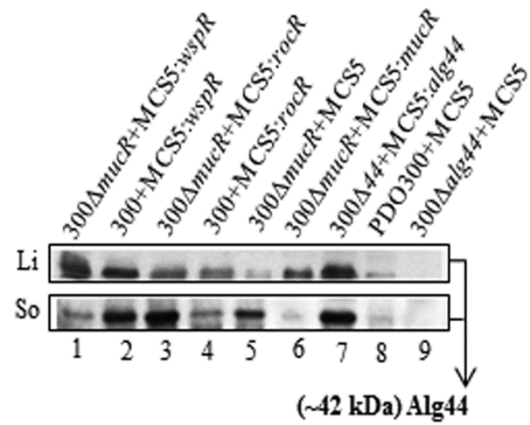


Figure 4. Alg44 stability is independent of c-di-GMP. In envelope fractions of planktonic (Li: liquid) and biofilm (So: solid) cells and in the presence and/or absence of WspR (generating c-di-GMP) (lanes 1,2) and RocR (degrading c-di-GMP) (lanes 3,4) and MucR (alginate biosynthesis-associated c-di-GMP regulator) (lanes 5,6) Alg44 was detected using immunoblotting with anti-Alg44 antibodies. Lanes 7-9 show negative and positive controls. 300: PDO300; MCS5:pBBR1MCS-5.

Figure 5. Bacterial cellulose synthase-associated autoinhibiting mechanism does not play a role in alginate polymerization.

(A) *In silico* fusion of Alg8-PilZ_{Alg44} was modeled using Phyre2 server. In this model our fusion protein had the highest homology (confidence 100%; coverage 93%) with BcsA glycosyltransferase from cellulose synthase complex whose C-terminal PilZ domain was previously proposed to localize adjacent to the catalytic site inducing a local conformational change upon binding to c-di-GMP to eliminate salt bridge bond formed between R580 (of PilZ domain's RxxxR motif) and E371 allowing the substrate to access the catalytic site (2). (B) In this model, the gray barrel-shaped structure is modeled as PilZ domain facing the catalytic site of Alg8. Highly conserved amino acids (blue sticks) before and after proposed functional residues (red sticks) known as the signature motif of GT-2 family members, were identified in a similar position to that of BcsA and which could form a salt bridge with R residues of PilZ_{Alg44} domain's RxxxR motif. (C) Pairwise alignment of Alg8-BcsA shows three candidates (E322, H323 and E326) potentially involved in salt bridge formation and which were replaced by alanine, respectively, in order to assess their role in salt bridge formation. (D) Alginate quantification of PDO300 Δ alg8, PDO300 Δ alg44 and PDO300 Δ alg8 Δ alg44 transformants with plasmids harboring respective site-specific mutants of *alg8* and *alg44* with (+) and without (-) *rocR* gene. Alg8's mutated residue which positively responded to c-di-GMP level alteration by RocR is labeled with asterisk. This experiment was conducted in triplicates and mean values plus standard deviation are shown. 300:PDO300; ND: Not detectable; MCS5: pBBR1MCS-5.

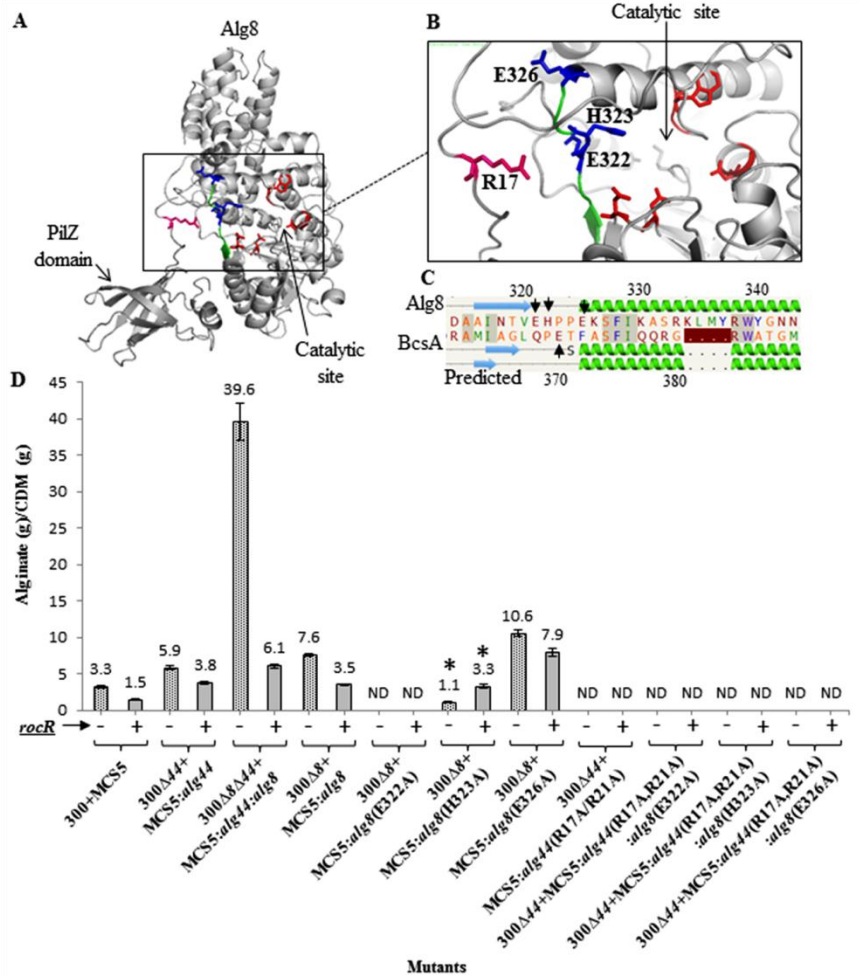


Figure 6. Impact of putative alginate polymerase subunits on alginate polymerase activity, alginate polymerization and composition and correlation between polymerization and modification. (A) The values of molar fraction of G residue (F_G), acetylation degrees (Ac.%), mean molecular weights (Mw) and alginate yield are aligned with the strains producing the respective alginates. (B) Correlation between degree of acetylation, epimerization and molecular weight of alginate. Presumable features (No. 1-11) show protein complexes constituted by Alg8, Alg44, AlgG and AlgX (cf. legend on top left corner of plot). The subunit produced upon *in trans* complementation is shown as darker shape(s). Inactive AlgX(S269A) and AlgG(D324A) are labeled as (A) and (E), respectively. The length of various alginates (PD) with respect to acetylation (Ac%) and epimerization (F_G) degrees are presented and proportionally illustrated for each feature. (C) The amount of alginate (yield) produced by the various *P. aeruginosa* PDO300 strains. Cells were grown on solid media and the amount of alginate is given in grams of alginate per gram of cellular dry mass (CDM). This experiment was conducted in triplicates and mean values plus standard deviation are shown. 300: PDO300; MCS5: pBBR1MCS-5; wt: wild-type; PD: polymerization degree; ND: not detectable; OM: outer membrane; CM: cytoplasmic membrane.

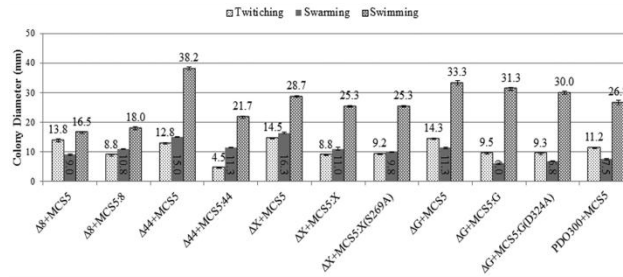
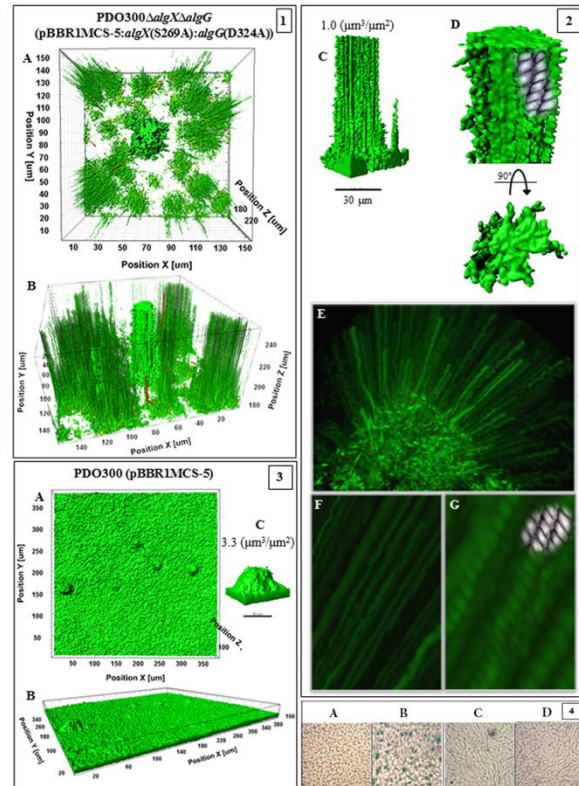


Figure 7. Impact of alginates on motility of *P. aeruginosa*. Twitching, swarming and swimming was assessed in triplicates on 1%, 0.5% and 0.3% agar plates, respectively, and after incubation at 30 °C for 18-24 h. The mean of colony diameter values \pm standard deviation errors are graphed.

Figure 8. Biofilm architecture of mutant producing non-epimerized and non-acetylated alginates and wild-type. This figure shows biofilm formation and architecture of the mutants PDO300 Δ *algX* Δ *algG*(pBBR1MCS-5:*algX*(S269A):*algG*(D324A)) (frame 1, 2) and PDO300 (pBBR1MCS-5) (frame 3). In all frames A, B and C shows respectively top view, side views and a representative of typical highly structured cell communities for that mutant with biovolume per area ($\mu\text{m}^3/\mu\text{m}^2$) ratio. Biofilm architecture visualized for mutant producing non-acetylated poly-M alginate was remarkably different from other applied mutants. Viscoelastic property of this alginate was found in the fourth group of MSD plot (the lowest values but higher than acetylated alginate). Affected by alginate properties, emerging biofilm consists of very narrow but long elevated microcolonies representing longitudinal cell trails or strips indicating stigmergic self-organization and adaptation of cells in weak matrices. Frame 2D-G represents close side and top views of one of the microcolonies and cell trails and cell-cell interactions in each cell trail are depicted in sketches. Wild-type biofilm architecture is presented in frame 3. Frame 4 shows micrographs (40X magnification) of the edge (A, C) and surface (B, D) of mucoid colonies of PDO300 (pBBR1MCS-5) (A, B) and PDO300 Δ *algX* Δ *algG*(pBBR1MCS-5:*algX*(S269A):*algG*(D324A)) (C, D) forming a thin layer on PIA medium after incubation at 37°C for 18 h. Organization of cells of PDO300 Δ *algX* Δ *algG*(pBBR1MCS-5:*algX*(S269A):*algG*(D324A)) mutant showed linear filamentous aggregation pattern.



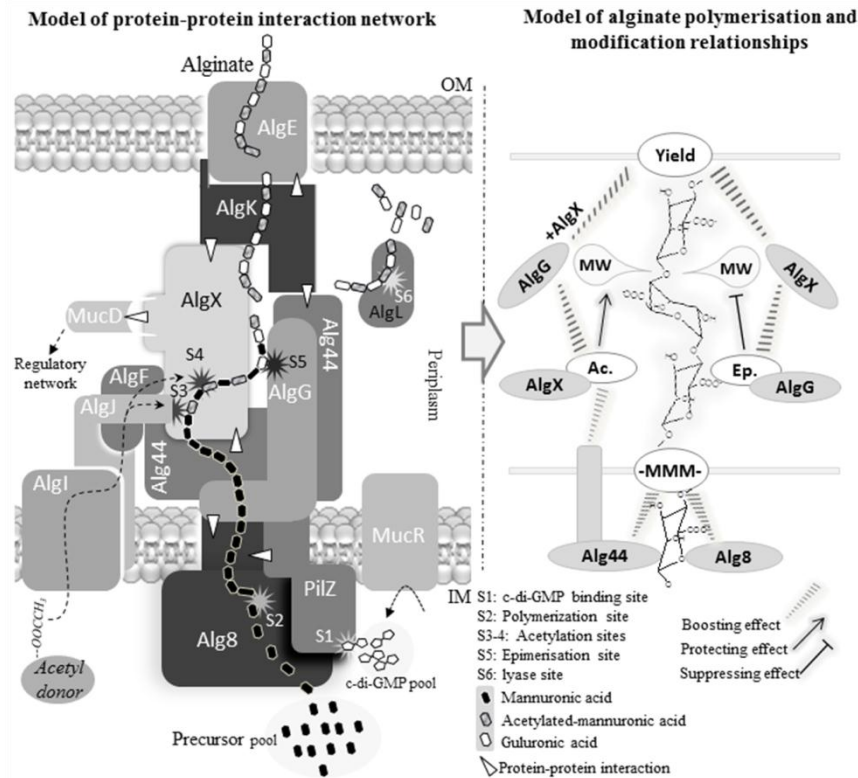


Figure 9. A new proposed model of alginate biosynthesis machinery complex and interactive performances of protein functionality over alginate polymerization, acetylation, epimerization and length determination. Based on experimental results obtained in the current study, functional and physical interaction of subunits (left side of figure) were modeled into a multiprotein complex. In this model different binary interactions are marked with white triangles. Our finding of Alg8-Alg44 and Alg44-AlgK interactions together with previously discovered interaction of AlgK-AlgE (1) constitute the periplasmic part of the multiprotein complex connecting the cytoplasmic membrane with the outer membrane. The model also includes the following interactions Alg44-AlgX, Alg8-AlgG, MucD-AlgX-AlgK, (1, 3) in support of the periplasmic scaffold guiding nascent alginate for translocation and secretion. This model shows alginate production is positively regulated by c-di-GMP binding to Alg44 interacting (* site 1 (S1)) targeting catalytic site of Alg8 polymerase (*S2) through an unknown mechanism. Then translocation across periplasmic scaffold is coupled with interactive functional performances of modification events and proteins (right side of model) for alginate length regulation and a series of associated modification events (*S 3-5). AlgL is responsible for degrading misguided alginate accumulating in periplasm (site 6). MucD protein links the complex with the posttranslational alginate regulatory network via an interaction with AlgX.

Supplemental Tables and Figures

Table S1. Strains and plasmids used in this study

Strains and plasmids	Description	Source or reference
Strains		
<i>P. aeruginosa</i>		
PDO300	<i>mucA22</i> isogenic mutant derived from PAO1, Alg ⁺	(1)
PDO300Δ <i>alg8</i>	Isogenic <i>alg8</i> deletion mutant derived from PDO300, Alg ⁻	(2)
PDO300 Δ <i>alg44</i>	Isogenic <i>alg44</i> deletion mutant derived from PDO300, Alg ⁻	(3)
PDO300 Δ <i>alg8</i> Δ <i>alg44</i>	Isogenic <i>alg8</i> and <i>alg44</i> deletions mutant derived from PDO300, Alg ⁻	This study
PDO300 Δ <i>algG</i>	Isogenic <i>algG</i> deletion mutant derived from PDO300, Alg ⁻	This study
PDO300 Δ <i>algX</i>	Isogenic <i>algX</i> deletion mutant derived from PDO300, Alg ⁻	(4)
PDO300 Δ <i>algG</i> Δ <i>algX</i>	Isogenic <i>algG</i> and <i>algX</i> deletions mutant derived from PDO300, Alg ⁻	This study
PDO300 Δ <i>algG</i> Δ <i>alg44</i>	Isogenic <i>algG</i> and <i>alg44</i> deletions mutant derived from PDO300, Alg ⁻	This study
PDO300 Δ <i>algX</i> Δ <i>alg44</i>	Isogenic <i>algX</i> and <i>alg44</i> deletions mutant derived from PDO300, Alg ⁻	This study
PDO300 Δ <i>mucR</i>	Isogenic <i>mucR</i> deletion mutant derived from PDO300, Alg ⁻	(5)
<i>E. coli</i>		
Top10	Cloning strain; F ⁻ <i>mcrA</i> , Δ(<i>mrr-hsdRMS-mcrBC</i>), φ80 <i>lacZ</i> Δ <i>M15</i> , Δ <i>lacX74</i> , <i>recA1</i> , <i>araD139</i> , Δ(<i>araleu</i>)7697 <i>galU</i> , <i>galK</i> , <i>rpsL</i> (Str ^R), <i>endA1</i> , <i>nupG</i>	Invitrogen
XL1 Blue	Cloning strain; <i>ecA1</i> , <i>endA1</i> , <i>gyrA96</i> , <i>thi-1</i> , <i>hsdR17</i> , (r _K ⁻ , m _K ⁺), <i>supE44</i> , <i>relA1</i> , Δ(<i>lac-proAB</i>) [F ⁻ , <i>proAB</i> , <i>lacI</i> ^q , <i>lacZ</i> Δ <i>M15</i> , Tn10(<i>tet</i> ^r)]	(6)
S17-1	Donor strain in transconjugation; <i>thi-1</i> , <i>proA</i> , <i>hsdR17</i> (r _K ⁻ , m _K ⁺), <i>recA1</i> ; <i>tra</i> gene of plasmid RP4 integrated in chromosome	(7)
SM10	Donor strain for pFLP2 plasmid; <i>thi-1</i> , <i>thr-1</i> , <i>leuB6</i> , <i>supE44</i> , <i>tonA21</i> , <i>lacY1</i> , <i>recA</i> ::RP4-2-Tc::Mu Km ^r	(7)
BTH101	Protein-protein interaction strain; F ⁻ , <i>cya-99</i> , <i>araD139</i> , <i>galE15</i> , <i>galK16</i> , <i>rpsL1</i> (Sp ^R), <i>hsdR2</i> , <i>mcrA1</i> , <i>mcrB1</i>	Euromedex
Plasmids		
pBBR1MCS-5	Gm ^r ; broad-host-range vector; P _{lac}	(8)
pBBR1MCS-5: <i>alg8</i>	<i>Hind</i> III- <i>Pst</i> I fragment comprising <i>alg8</i> inserted into vector pBBR1MCS-5	(2)
pBBR1MCS-5: <i>alg8</i> -6his	Translational Alg8-hexahistidine tag fusion, inserted into vector pBBR1MCS-5	(9)
pBBR1MCS-5: <i>alg44</i>	<i>Hind</i> III- <i>Bam</i> HI fragment comprising <i>alg44</i> inserted into vector pBBR1MCS-5	(3)
pBBR1MCS-5: <i>alg44</i> (R21D)-6his	<i>Hind</i> III- <i>Bam</i> HI fragment comprising <i>alg44</i> encoding translational Alg44-hexahistidine tag fusion with site-directed mutagenesis R21A inserted into vector pBBR1MCS-5	This study

pBBR1MCS-5: <i>alg44</i> (R17A)	<i>Hind</i> III- <i>Bam</i> HI fragment comprising <i>alg44</i> encoding site-directed mutagenesis R17A inserted into vector pBBR1MCS-5	This study
pBBR1MCS-5: <i>alg44</i> (R21A)	<i>Hind</i> III- <i>Bam</i> HI fragment comprising <i>alg44</i> encoding site-directed mutagenesis R21A inserted into vector pBBR1MCS-5	This study
pBBR1MCS-5: <i>alg44</i> (R17A, R21A)	<i>Hind</i> III- <i>Bam</i> HI fragment comprising <i>alg44</i> encoding site-directed mutagenesis R17A and R21A inserted into vector pBBR1MCS-5	This study
pBBR1MCS-5: <i>alg44</i> (R17A, R21A): <i>rocR</i>	<i>Hind</i> III- <i>Bam</i> HI fragment comprising <i>alg44</i> encoding site-directed mutagenesis R17A and R21A and <i>Xba</i> I- <i>Sac</i> I fragment encoding RocR (PA3947) inserted into vector pBBR1MCS-5	This study
pBBR1MCS-5: <i>alg44</i> (Δ 40-74aa _{PilZ})-6his	<i>Hind</i> III- <i>Bam</i> HI fragment comprising <i>alg44</i> encoding translational Alg44 with N-terminal oligonucleotide deletion (residues 40-74) inserted into vector pBBR1MCS-5	This study
pBBR1MCS-5: <i>alg44</i> (Δ 364-389aa)-6his	<i>Hind</i> III- <i>Bam</i> HI fragment comprising <i>alg44</i> encoding translational Alg44 with C-terminal oligonucleotide deletion (residues 364-389) inserted into vector pBBR1MCS-5	This study
pBBR1MCS-5: <i>alg44</i> -6his	Translational Alg44-hexahistidine tag fusion, inserted into vector pBBR1MCS-5	This study
pBBR1MCS-5: <i>alg44:alg8</i>	<i>Cla</i> I- <i>Hind</i> III fragment comprising <i>alg44</i> and <i>Hind</i> III- <i>Pst</i> I fragment comprising <i>alg8</i> inserted into vector pBBR1MCS-5	This study
pBBR1MCS-5: <i>alg8</i> (E322A)	<i>Hind</i> III- <i>Pst</i> I fragment comprising <i>alg8</i> encoding site-directed mutagenesis E322A inserted into vector pBBR1MCS-5	This study
pBBR1MCS-5: <i>alg8</i> (E322A): <i>rocR</i>	<i>Hind</i> III- <i>Pst</i> I fragment comprising <i>alg8</i> encoding site-directed mutagenesis E322A and <i>Xba</i> I- <i>Sac</i> I fragment comprising RocR(PA3947) inserted into vector pBBR1MCS-5	This study
pBBR1MCS-5: <i>alg8</i> (H323A)	<i>Hind</i> III- <i>Pst</i> I fragment comprising <i>alg8</i> encoding site-directed mutagenesis H323A inserted into vector pBBR1MCS-5	This study
pBBR1MCS-5: <i>alg8</i> (H323A): <i>rocR</i>	<i>Hind</i> III- <i>Pst</i> I fragment comprising <i>alg8</i> encoding site-directed mutagenesis H323A and <i>Xba</i> I- <i>Sac</i> I fragment comprising RocR(PA3947) inserted into vector pBBR1MCS-5	This study
pBBR1MCS-5: <i>alg8</i> (E326A)	<i>Hind</i> III- <i>Pst</i> I fragment comprising <i>alg8</i> encoding site-directed mutagenesis E326A inserted into vector pBBR1MCS-5	This study
pBBR1MCS-5: <i>alg8</i> (E326A): <i>rocR</i>	<i>Hind</i> III- <i>Pst</i> I fragment comprising <i>alg8</i> encoding site-directed mutagenesis E326A and <i>Xba</i> I- <i>Sac</i> I fragment comprising RocR(PA3947) inserted into vector pBBR1MCS-5	This study
pBBR1MCS-5: <i>alg44</i> (R17A): <i>alg8</i> (E322A)	<i>Cla</i> I- <i>Hind</i> III fragment comprising <i>alg44</i> encoding site-directed mutagenesis R17A and <i>Hind</i> III- <i>Pst</i> I fragment comprising <i>alg8</i> encoding site-directed mutagenesis E322A inserted into vector pBBR1MCS-5	This study
pBBR1MCS-5: <i>alg44</i> (R21A): <i>alg8</i> (E322A)	<i>Cla</i> I- <i>Hind</i> III fragment comprising <i>alg44</i> encoding site-directed mutagenesis R21A and <i>Hind</i> III- <i>Pst</i> I fragment comprising <i>alg8</i> encoding site-directed mutagenesis E322A inserted into vector pBBR1MCS-5	This study
pBBR1MCS-5: <i>alg44</i> (R17A,R21A): <i>alg8</i> (E322A)	<i>Cla</i> I- <i>Hind</i> III fragment comprising <i>alg44</i> encoding site-directed mutagenesis R17A and R21A and <i>Hind</i> III- <i>Pst</i> I fragment comprising <i>alg8</i> encoding site-directed mutagenesis E322A	This study

	inserted into vector pBBR1MCS-5	
pBBR1MCS-5: <i>alg44</i> (R17A,R21A): <i>alg8</i> (E322A): <i>rocR</i>	<i>Cla</i> I- <i>Hind</i> III fragment comprising <i>alg44</i> encoding site-directed mutagenesis R17A and R21A and <i>Hind</i> III- <i>Pst</i> I fragment comprising <i>alg8</i> encoding site-directed mutagenesis E322A and <i>Xba</i> I- <i>Sac</i> I fragment encoding RocR(PA3947) inserted into vector pBBR1MCS-5	This study
pBBR1MCS-5: <i>alg44</i> (R17A): <i>alg8</i> (H323A)	<i>Cla</i> I- <i>Hind</i> III fragment comprising <i>alg44</i> encoding site-directed mutagenesis R17A and <i>Hind</i> III- <i>Pst</i> I fragment comprising <i>alg8</i> encoding site-directed mutagenesis H323A inserted into vector pBBR1MCS-5	This study
pBBR1MCS-5: <i>alg44</i> (R21A): <i>alg8</i> (H323A)	<i>Cla</i> I- <i>Hind</i> III fragment comprising <i>alg44</i> encoding site-directed mutagenesis R21A and <i>Hind</i> III- <i>Pst</i> I fragment comprising <i>alg8</i> encoding site-directed mutagenesis E323A inserted into vector pBBR1MCS-5	This study
pBBR1MCS-5: <i>alg44</i> (R17A,R21A): <i>alg8</i> (H323A)	<i>Cla</i> I- <i>Hind</i> III fragment comprising <i>alg44</i> encoding site-directed mutagenesis R17A and R21A and <i>Hind</i> III- <i>Pst</i> I fragment comprising <i>alg8</i> encoding site-directed mutagenesis H323A inserted into vector pBBR1MCS-5	This study
pBBR1MCS-5: <i>alg44</i> (R17A,R21A): <i>alg8</i> (H323A): <i>rocR</i>	<i>Cla</i> I- <i>Hind</i> III fragment comprising <i>alg44</i> encoding site-directed mutagenesis R17A and R21A and <i>Hind</i> III- <i>Pst</i> I fragment comprising <i>alg8</i> encoding site-directed mutagenesis H323A and <i>Xba</i> I- <i>Sac</i> I fragment encoding RocR(PA3947) inserted into vector pBBR1MCS-5	This study
pBBR1MCS-5: <i>alg44</i> (R17A): <i>alg8</i> (E326A)	<i>Cla</i> I- <i>Hind</i> III fragment comprising <i>alg44</i> encoding site-directed mutagenesis R17A and <i>Hind</i> III- <i>Pst</i> I fragment comprising <i>alg8</i> encoding site-directed mutagenesis E326A inserted into vector pBBR1MCS-5	This study
pBBR1MCS-5: <i>alg44</i> (R21A): <i>alg8</i> (E326A)	<i>Cla</i> I- <i>Hind</i> III fragment comprising <i>alg44</i> encoding site-directed mutagenesis R21A and <i>Hind</i> III- <i>Pst</i> I fragment comprising <i>alg8</i> encoding site-directed mutagenesis E326A inserted into vector pBBR1MCS-5	This study
pBBR1MCS-5: <i>alg44</i> (R17A,R21A): <i>alg8</i> (E326A)	<i>Cla</i> I- <i>Hind</i> III fragment comprising <i>alg44</i> encoding site-directed mutagenesis R17A and R21A and <i>Hind</i> III- <i>Pst</i> I fragment comprising <i>alg8</i> encoding site-directed mutagenesis E326A inserted into vector pBBR1MCS-5	This study
pBBR1MCS-5: <i>alg44</i> (R17A,R21A): <i>alg8</i> (E326A): <i>rocR</i>	<i>Cla</i> I- <i>Hind</i> III fragment comprising <i>alg44</i> encoding site-directed mutagenesis R17A and R21A and <i>Hind</i> III- <i>Pst</i> I fragment comprising <i>alg8</i> encoding site-directed mutagenesis E326A and <i>Xba</i> I- <i>Sac</i> I fragment encoding RocR(PA3947) inserted into vector pBBR1MCS-5	This study
pBBR1MCS-5: <i>algG</i>	<i>Bam</i> HI- <i>Xba</i> I fragment comprising <i>algG</i> inserted into vector pBBR1MCS-5	This study
pBBR1MCS-5: <i>algG</i> (D324A)	<i>Bam</i> HI- <i>Xba</i> I fragment comprising <i>algG</i> encoding site-directed mutagenesis D324A inserted into vector pBBR1MCS-5; mannuronic acid(M)-epimerase activity	This study
pBBR1MCS-5: <i>algG</i> -6his	Translational AlgG-hexahistidine tag fusion, inserted into vector pBBR1MCS-5	This study
pBBR1MCS-5: <i>algX</i>	<i>Hind</i> III- <i>Bam</i> HI fragment comprising <i>algX</i>	

	inserted into vector pBBR1MCS-5	
pBBR1MCS-5: <i>algX</i> -6his	Translational AlgX-hexahistidine tag fusion, inserted into vector pBBR1MCS-5	This study
pBBR1MCS-5: <i>algX</i> (S269A)	<i>Hind</i> III- <i>Bam</i> HI fragment comprising <i>algX</i> encoding site-directed mutagenesis S269A inserted into vector pBBR1MCS-5; Acetyltransferase activity	This study
pBBR1MCS-5: <i>algX:algG</i>	<i>Hind</i> III- <i>Bam</i> HI fragment comprising <i>algX</i> and <i>Bam</i> HI- <i>Xba</i> I fragment comprising <i>algG</i> inserted into vector pBBR1MCS-5	This study
pBBR1MCS-5: <i>algX</i> (S269A): <i>algG</i> (D324A)	<i>Hind</i> III- <i>Bam</i> HI fragment comprising <i>algX</i> encoding site-directed mutagenesis S269A and <i>Bam</i> HI- <i>Xba</i> I fragment comprising <i>algG</i> encoding site-directed mutagenesis D324A inserted into vector pBBR1MCS-5; M-epimerase activity, Acetyltransferase activity	This study
pBBR1MCS-5: <i>alg44:algG</i>	<i>Cla</i> I- <i>Bam</i> HI fragment comprising <i>alg44</i> and <i>Bam</i> HI- <i>Xba</i> I fragment comprising <i>algG</i> inserted into vector pBBR1MCS-5	This study
pBBR1MCS-5: <i>algX:alg44</i>	<i>Cla</i> I- <i>Hind</i> III fragment comprising <i>algX</i> and <i>Hind</i> III- <i>Bam</i> HI fragment comprising <i>alg44</i> inserted into vector pBBR1MCS-5	This study
pBBR1MCS-5: <i>mucR</i>	<i>Kpn</i> I- <i>Cla</i> I fragment comprising <i>mucR</i> inserted into vector pBBR1MCS-5	(5)
pBBR1MCS-5: <i>wspR</i>	<i>Xba</i> I- <i>Sac</i> I fragment comprising <i>wspR</i> inserted into vector pBBR1MCS-5	(5)
pBBR1MCS-5: <i>rocR</i>	<i>Xba</i> I- <i>Sac</i> I fragment comprising <i>rocR</i> inserted into vector pBBR1MCS-5	(5)
pEX100T	Ap ^r Cb ^r , gene replacement vector containing <i>sacB</i> gene for counterselection	(10)
pEX100T:Δ <i>alg8</i> Gm	Ap ^r Cb ^r , Gm ^r , vector pEX100T with <i>Sma</i> I-inserted <i>alg8</i> deletion construct	(2)
pEX100T:Δ <i>alg44</i> Gm	Ap ^r Cb ^r , Gm ^r , vector pEX100T with <i>Sma</i> I-inserted <i>alg44</i> deletion construct	(3)
pEX100T:Δ <i>algGG</i> Gm	Ap ^r Cb ^r , Gm ^r , vector pEX100T with <i>Sma</i> I-inserted <i>algG</i> deletion construct	This study
pFLP2	Ap ^r Cb ^r ; broad-host-range vector encoding Flp recombinase	(10)
pGEM-T Easy	Cloning vector; Amp ^r ; T-overhang cloning	Promega
pGEM-T Easy: <i>alg44</i> -6his	A-tailed fragment encoding C-terminally hexahistidine-tagged Alg44 inserted into pGEM-T Easy	This study
pGEM-T Easy: <i>alg44</i> (Δ364-389aa)		This study
pGEM-T Easy: <i>alg8</i> -6his	A-tailed fragment encoding C-terminally hexahistidine-tagged Alg8 inserted into pGEM-T Easy used for sequencing	This study
pGEM-T Easy: <i>algX</i> -6his	A-tailed fragment encoding C-terminally hexahistidine-tagged AlgX inserted into pGEM-T Easy used for sequencing	This study
pGEM-T Easy: <i>algG</i> -6his	A-tailed fragment encoding C-terminally hexahistidine-tagged AlgG inserted into pGEM-T Easy used for sequencing	This study
Mini-CTX-lacZ	Chromosomal integration vector at the CTX phage <i>att</i> site on the <i>P. aeruginosa</i> chromosome, Tc ^r	(11)
Mini-CTX: <i>Palg44</i> -6his	<i>Pst</i> I- <i>Hind</i> III fragment encoding alginate operon promoter (<i>PalgD</i>) and <i>Hind</i> III- <i>Bam</i> HI fragment encoding C-terminally hexahistidine-tagged Alg44 inserted into vector Mini-CTX-lacZ	This study

Mini-CTX: <i>Palg8</i> -6his	<i>Pst</i> I- <i>Hind</i> III fragment encoding alginate operon promoter (<i>PalgD</i>) and <i>Hind</i> III- <i>Bam</i> HI fragment encoding C-terminally hexahistidine-tagged Alg8 inserted into vector Mini-CTX-lacZ	This study
Mini-CTX: <i>PalgG</i> -6his	<i>Pst</i> I- <i>Hind</i> III fragment encoding alginate operon promoter (<i>PalgD</i>) and <i>Hind</i> III- <i>Bam</i> HI fragment encoding C-terminally hexahistidine-tagged AlgG inserted into vector Mini-CTX-lacZ	This study
Mini-CTX: <i>PalgX</i> -6his	<i>Pst</i> I- <i>Hind</i> III fragment encoding alginate operon promoter (<i>PalgD</i>) and <i>Hind</i> III- <i>Bam</i> HI fragment encoding C-terminally hexahistidine-tagged AlgX inserted into vector Mini-CTX-lacZ	This study
pKNT25	3.4-kb plasmid allowing C-terminal protein fusion to T25 fragment; Kan ^r	Euromedex
pKNT25: <i>alg8</i>	<i>Hind</i> III- <i>Bam</i> HI fragment comprising <i>alg8</i> (Δ stop) cloned into pKNT25 upstream of T25 fragment	This study
pKNT25: <i>alg44</i>	<i>Hind</i> III- <i>Bam</i> HI fragment comprising <i>alg44</i> (Δ stop) cloned into pKNT25 upstream of T25 fragment	This study
pKT25-zip	Derivative of pKT25, having an leucine zipper motif of GCN4 fused in frame to the C-terminal end of CyaA _{T25} ; Kan ^r	Euromedex
pUT18	3.0-kb plasmid allowing C-terminal protein fusion to T18 fragment; Amp ^r	Euromedex
pUT18: <i>alg8</i>	<i>Hind</i> III- <i>Bam</i> HI fragment comprising <i>alg8</i> (Δ stop) cloned into pUT18 upstream of T18 fragment	This study
pUT18: <i>alg44</i>	<i>Hind</i> III- <i>Bam</i> HI fragment comprising <i>alg44</i> (Δ stop) cloned into pUT18 upstream of T18 fragment	This study
pUT18C-zip	Derivative of pUT18, having an leucine zipper motif of GCN4 fused in frame to the C-terminal end of CyaA _{T18} ; Amp ^r	Euromedex

Figure S1: NMR spectra

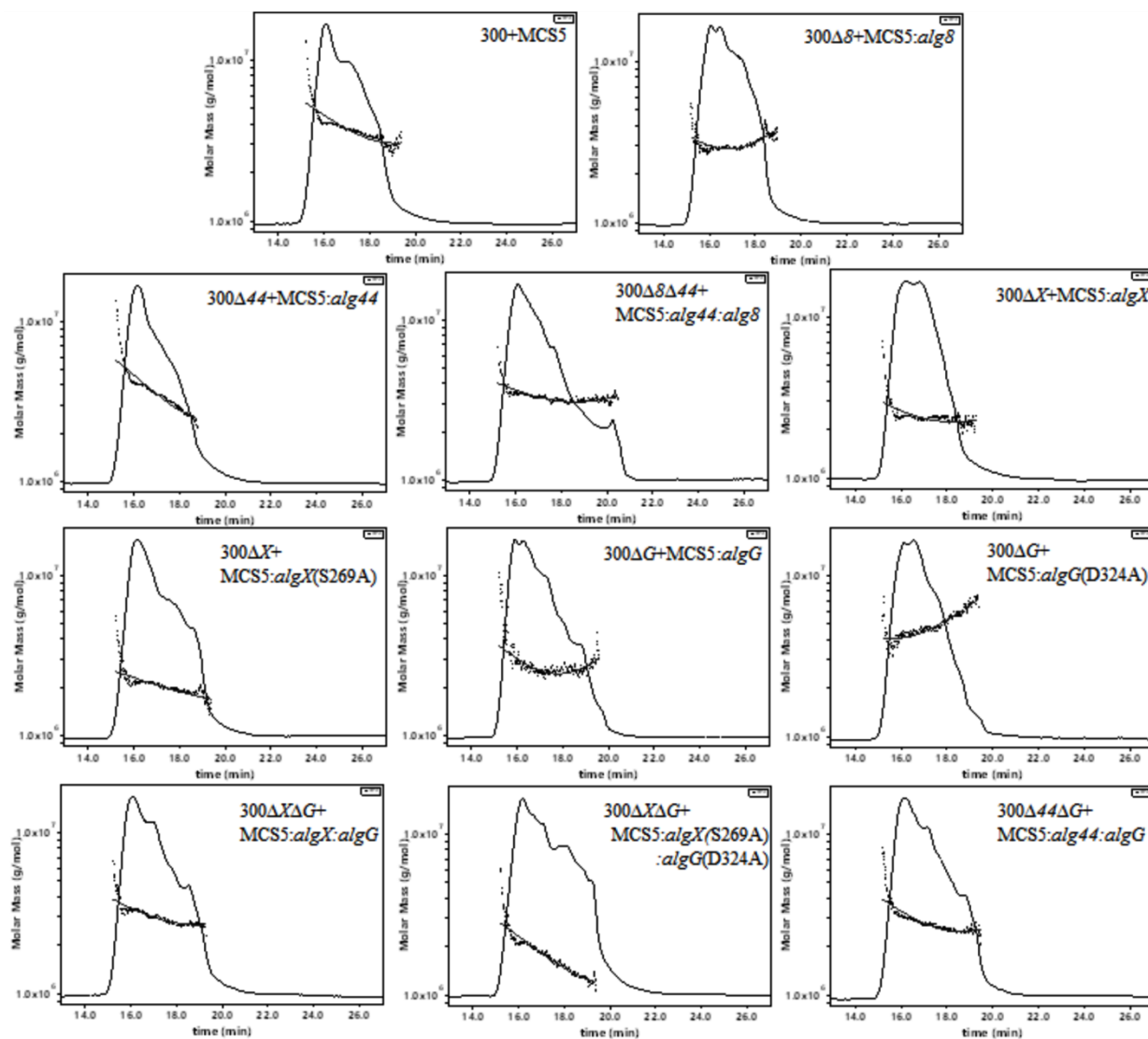


Figure S2- Plots showed molar mass of alginate samples versus time analyzed using SEC-MALLS. 300:PDO300; MCS5:pBBR1MCS-5.

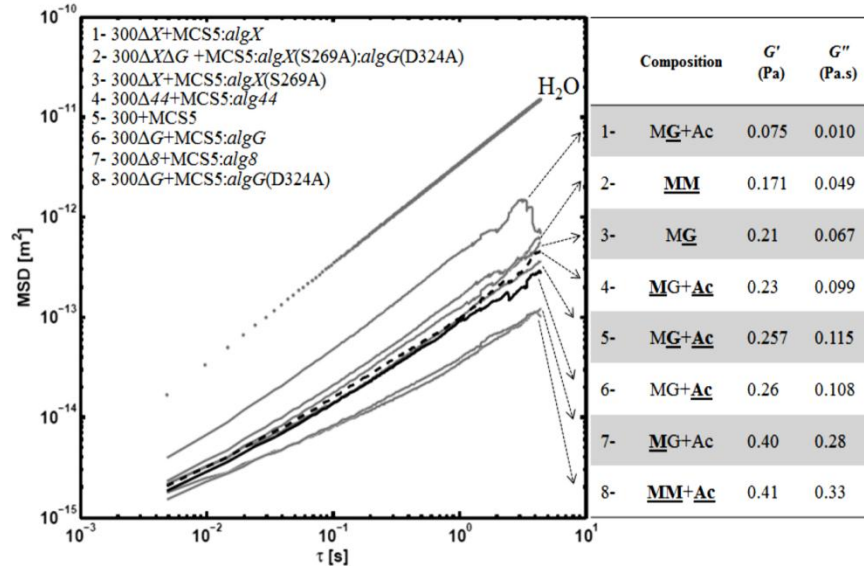


Figure S3. Viscoelastic property of alginates was impacted by molecular weight and modifications. The plot of MSD versus time shows distribution of alginate viscoelastic properties in four distinct regions. Alginates composition and viscoelasticity moduli (G' : elastic, G'' : viscous) are presented next to the plot. Bold and underlined letters indicate the predominance of mannuronate (M)/guluronate (G) molar fraction or acetylation (Ac) degree among all analyzed alginates. 300: PDO300; MCS5: pBBR1MCS-5.

Figure S4. Biofilm architecture of mutants producing acetylated and non-acetylated alginates. This figure shows biofilm formation and architecture of the mutants PDO300 Δ *algX*(pBBR1MCS-5:*algX*) (frames 1, 2), PDO300 Δ *algX*(pBBR1MCS-5:*algX*(S269A)) (frame 3) which produce acetylated and non-acetylated alginates, respectively, and PDO300 Δ *algX*(pBBR1MCS-5) (frame 4) with no alginate production. Frames A, B and C shows top view, side views and a representative of typical highly structured cell community respectively. The cell community dimensions are provided as $\mu\text{m}^3/\mu\text{m}^2$.

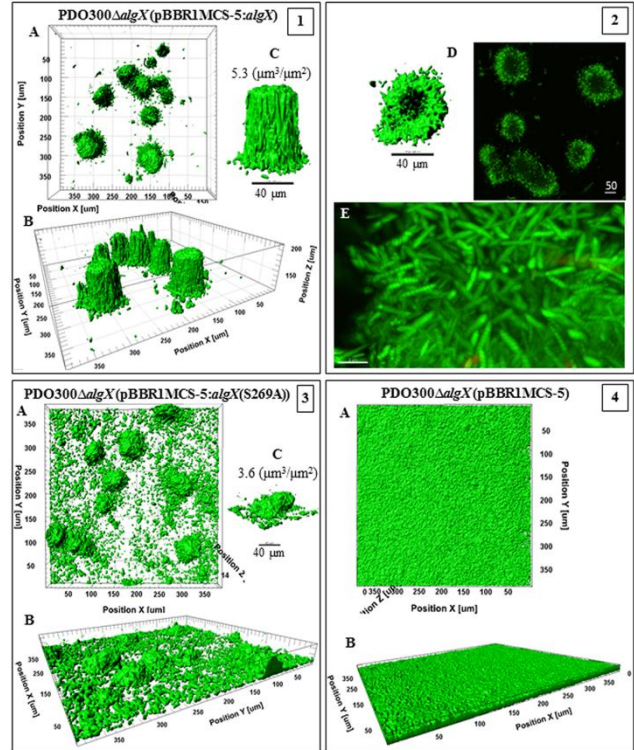


Figure S5. Biofilm architecture of mutants producing epimerized and non-epimerized alginates. This figure shows biofilm formation and architecture of the mutants

PDO300 Δ *algG*(pBBR1MCS-5:*algG*) (frame 1),

PDO300 Δ *algG*(pBBR1MCS-5:*algG*(D324A)) (frame 3,4) which produce, respectively, epimerized (poly-MG) and non-epimerized (poly-M) alginates and

PDO300 Δ *algG*(pBBR1MCS-5) (frame 2) with no alginate production. In all frames A,

B and C shows respectively top view, side views and a representative of typical highly structured cell communities for that mutant with biovolume per area ($\mu\text{m}^3/\mu\text{m}^2$) ratio. In

frame 3, poly-M alginate-based biofilm is highly developed than polyMG alginate-based in frame 1, presenting larger biovolume and biovolume per area ratio. Cells of both mutant covered entire cover slide surface. Frame 4D, E

represent the architecture of poly-M alginate-based microcolonies in which two adjacent structures are connected with horizontal appendages and free-cell void cavities channeled underneath of microcolonies. Frame 4D shows 6 different slices of microcolonies with connected structure at the middle of figures surrounded by free-cell and matrix areas. Frame 2 represents homogenous cell community of non-mucoid mutant without highly structured architecture.

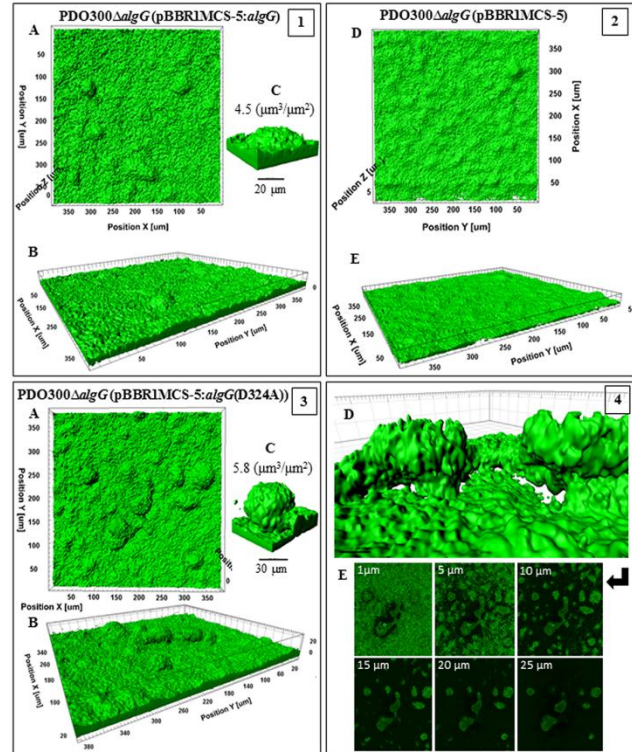


Figure S6. Biofilm architecture of mutant producing high mannuronate molar fraction and M-block. This figure shows biofilm formation and architecture of the mutants PDO300 Δ *alg8* (pBBR1MCS-5:*alg8*) (frame 1) and PDO300 Δ *alg44* (pBBR1MCS-5:*alg44*) (frame 3) and non-mucoid mutants (frames 2, 4). PDO300 (pBBR1MCS-5) (frame 3). In all frames A, B and C shows respectively top view, side views and a representative of typical highly structured cell communities for that mutant with biovolume per area ($\mu\text{m}^3/\mu\text{m}^2$) ratio. Both mutants produce alginates with highest degree of M-block occurrence but very different degree of acetylation. PDO300 Δ *alg44* (pBBR1MCS-5:*alg44*) (frame 3) which produce highly acetylated alginate established a very dense and highly developed and larger microcolonies than PDO300 Δ *alg8* (pBBR1MCS-5:*alg8*) (frame 1). One explanation for this significance difference is the presence of additional copy of Alg44 which senses c-di-GMP which is a common secondary messenger in the cells governing physiological condition of cells during colonization. However, non-mucoid mutants did not establish highly structured biofilm and microcolonies.

